Austrian Journal of Earth Sciences | Volume 108/1 | 73 - 90 | Vienna | 2015

# Prograde Permo-Triassic metamorphic HT/LP assemblages from the Austroalpine Jenig Complex (Carinthia, Austria)

Ralf SCHUSTER[1)*], Peter TROPPER[2)], Erwin KRENN[3)], Friedrich FINGER[3)], Wolfgang FRANK[4)] & Rudolf PHILIPPITSCH[5)]

[1)] Geologische Bundesanstalt, Neulinggasse 38, A-1030 Wien, Austria;

[2)] Institut für Mineralogie und Petrographie, Fakultät für Geo- und Atmosphärenwissenschaften, Universität Innsbruck, Innrain 52f, A-6020 Innsbruck, Austria;

[3)] Fachberich Materialforschung und Physik, Universität Salzburg, Hellbrunnerstrasse 34, 5020 Salzburg, Austria;

[4)] Köhldorfergasse 26, 3040 Neulengbach, Austria;

[5)] Jadersdorf 18, 9620 Hermagor, Austria;

[*)] Corresponding author, ralf.schuster@geologie.ac.at

DOI: 10.17738/ajes.2015.0005

KEYWORDS

metamorphism
geochronology
Austroalpine
Permian

## Abstract

In this study the *P-T-t* evolution of the Jenig Complex (Austroalpine) which is part of the crystalline basement of the Gail valley (Carinthia/Austria) has been investigated. The Jenig Complex covers an area of about 1.5 km² on the slopes of the valley directly north of Jenig. It consists of mica schists, quarzitic mica schists, quartzites and paragneisses. Intercalations of up to a few meters thick garnet- and hornblende-bearing quartzschists as well as andalusite-bearing quartz veins are scarce. The mica schists are Al-rich metapelites and characterized by the following mineral assemblage: St, Grt, And, Bt, Ms, Pl, Qtz, Chl, Ilm, graphite, Czoi, Mz, Ap, Zrn, Tur. Garnet and staurolite show a continuous chemical zoning all other minerals are chemically unzoned. *P-T* calculations for three samples containing the assemblage garnet + andalusite + biotite + plagioclase + muscovite + quartz are ranging from 450 to 530°C and 0.24 to 0.42 GPa. EMS-dating of monazite yielded 275±25 Ma, whereas a Sm-Nd isochron, including four whole rocks and three garnet fractions yielded 254±8 Ma. A Sm-Nd age of a staurolite is 231±4 Ma. The final cooling below 400°C and 300°C occurred at 205±5 Ma and 185±5 Ma respectively, based on Ar-Ar muscovite and Rb-Sr biotite ages. Due to this data the assemblages of the Jenig Complex formed during the Permo-Triassic extensional event and cooled down in the Late Triassic to Early Jurassic. The Jenig Complex forms a tectonic slice which developed during Jurassic sinistral strike-slip tectonics, Cretaceous folding and was finally exhumed by shearing along the Periadriatic fault.

Die vorliegende Arbeit behandelt die *P-T-t* Entwicklung des Jenig-Komplex (Ostalpin), der einen Teil des Kristallins im Gailtales (Kärnten/Österreich) aufbaut. Der Jenig-Komplex nimmt eine Fläche von etwa 1,5 km² an den Nordhängen des Tales, direkt nördlich der Ortschaft Jenig ein. Er besteht aus Glimmerschiefern, quarzitischen Glimmerschiefern, Quarziten und Paragneisen. Weiter finden sich vereinzelt einige Meter mächtige Lagen von Grant und Hornblende-führenden Quarzschiefern sowie Andalusit-führende Quarzmobilisat-Gänge. Bei den Glimmerschiefer handelt es sich zum Teil um Al-reiche Metapelite, die durch folgende Mineralzusammensetzung gekennzeichnet sind: Staurolith, Grant, Andalusit, Biotit, Muskovit, Plagioklas, Quarz, Chlorit Ilmenit, Graphit, Klinozoisit Monazit, Zirkon und Turmalin. Granat und Staurolith zeigen kontinuierliche chemische Zonierungen, alle anderen Minerale sind chemisch homogen. *P-T* Bestimmungen an drei Proben, welche den Mineralbestand Granat + Andalusit + Biotit + Plagioklas + Muskovit +Quarz beinhalten, ergaben Gleichgewichtsbedingungen von 450 bis 530°C bei 0,24 bis 0,42 GPa. Datierungen von Monazit mit der EMS-Methode lieferten Alter von 275±25 Ma, während eine Sm-Nd Isochrone die vier Gesamtgesteine und drei Granatfraktionen beinhaltet ein Alter von 254±8 Ma ergab. Ein weiteres Sm-Nd Alter gemessen an Staurolith und Gesamtgestein liegt bei 231±4 Ma. Die Abkühlung der Gestein unter 400°C und 300°C geschah um 205±5 Ma beziehungsweise um 185±5 Ma, basierend auf Ar-Ar Muskovit und Rb-Sr Biotitaltern. Mit Bezug auf die Altersdaten entstanden die Mineralparagenesen im Jenig-Komplex während des Permotriassichen Extensions-Ereignisses und die Gesteine kühlten danach in der Obertrias und im Unterjura ab. Der Jenig-Komplex bildet eine Decke, welche sich während jurassischer Seitenverschiebungen und kretazischer Faltung bildete und später entlang des Periadriatischen Störungssystems an die Erdoberfläche exhumiert wurde.

## 1. Introduction

In the past decade a widespread Permo-Triassic high-pressure/low temperature (HT/LP) metamorphic imprint has been recognised in the Austroalpine unit (Schuster and Thöni 1995; Habler and Thöni 2001; Schuster et al. 2001, 2004; Schuster and Stüwe 2008; Thöni and Miller 2009). In most cases the Permo-Triassic assemblages have been identified within polymetamorphic rocks. Often they are overprinting Variscan assemblages, but more frequently they are overprinted by the eo-Alpine (Cretaceous) tectonothermal event. A typical example for the first case is the Strieden-Michelbach Complex in the Kreuzeck and Deferegger Mountains (Steidl et al. 2010). Examples for the second case are the Wölz-, Rappold- and Plankogel Complex (Habler and Thöni 2001; Gaidies et al. 2005; Bestl et al. 2009; Thöni and Miller 2009). Determination of the Permian *P-T* evolution in these units is much more difficult, because only relics of the HT-LP assemblage are preser-

ved. In most cases these relics are represented by garnet and some inclusions within the garnet, as well as andalusite or sillimanit and kyanite pseudomorphs of these minerals respectively.

However, as *P-T* paths can be studied best on rock samples which experienced one prograde metamorphic imprint, reliable geothermobarometric *P-T* data for the Permo-Triassic imprint are scarce. For this reason a lithological unit occurring on the northern slopes of the Gail valley (Carinthia/Austria) affected by the Permo-Triassic metamorphic imprint only is of special interest. In this paper mineral-rich metapelitic assemblages of this unit, which is referred to as the Jenig Complex in the following, are described in detail and their P-T-t evolution is highlighted based on petrological, structural, geochronological and geochemical data as well as geothermobarometric calculations. Further a review on the basement rocks of the Gail valley is given and discussed in the light of the new data.

## 2. Regional Geology

The Austroalpine unit represents the uppermost tectonic unit in the Eastern Alps (Fig. 1A). Since Palaeozoic times this piece

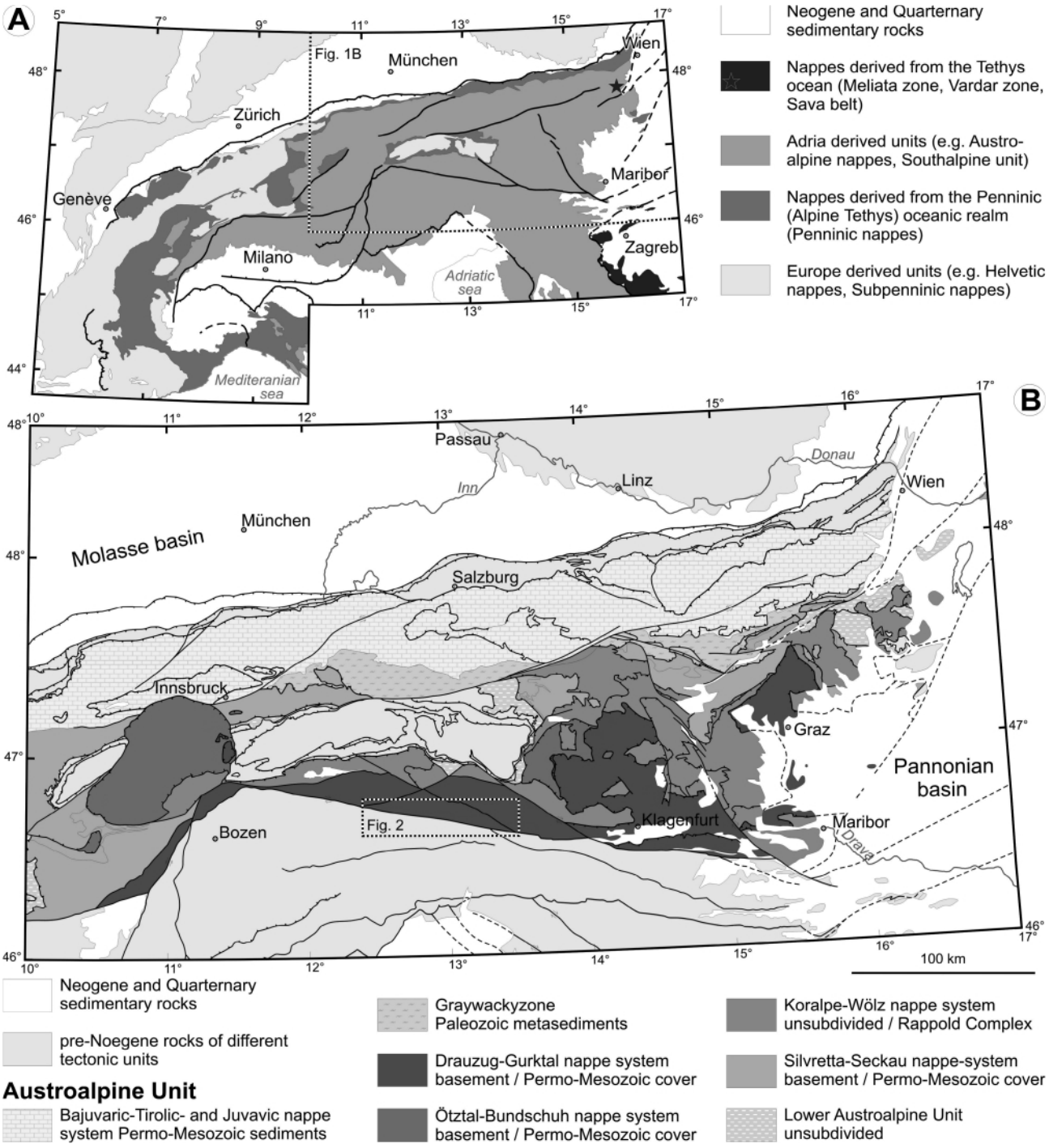


**Figure 1:** Overview maps (A) showing the paleogeographic origin of the main tectonic units of the Alps, and (B) the tectonic subdivision of the Austroalpine unit based on Schmid et al. (2004).

of continental crust was affected by several regional metamorphic and/or magmatic events (Neubauer et al. 1999; Hoinkes et al. 1999; Schuster et al. 2004). In the Ordovician a widespread magmatic event affected the recent Austroalpine nappes. A Late Devonian to Carboniferous imprint is related to the Variscan tectonothermal cycle and characterised by a clockwise P-T-t evolution. In Permo-Triassic time large parts of the Austroalpine units were affected by lithospheric extension and related HT/LP metamorphism (Schuster and Stüwe 2008). The eo-Alpine tectonothermal event in the Cretaceous is due to intracontinental shortening within the Austroalpine unit which formed the northernmost part of the Adriatic Plate at that time (Janák et al. 2004; Stüwe and Schuster, 2010). Finally in Oligocene to Miocene times a thermal influence of the Alpine metamorphic event, related to the subduction of the Penninic (Alpine Tethys) Ocean and the following collision of the European and the Adriatic plate can be recognized in some of the tectonically lowermost parts of the Austroalpine unit especially to the south of the Tauern Window. Individual Austroalpine units were affected differently by the events mentioned above. Most of them are polymetamorphic, but several experienced only one prograde overprint.

The Jenig Complex is part of Austroalpine crystalline basement outcropping directly to the north of the Periadriatic fault and the Southalpine unit. To the north this basement is overlain by locally occurring Carboniferous sequences and by Permo-Mesozoic sediments. Since Kober (1938) the crystalline basement, the Paleozoic rocks and the Permo-Mesozoic cover are denoted as the Drau range ("Drauzug"). The later forms a several 100 km long, WNW-ESE trending belt between the Drau river in the West and the city Varaždin in Croatia in the East. Due to its position along the Periadriatic fault the Drau range is characterised by highly tectonized WNW-WSE striking slices with different kinds of crystalline basement rocks and Permo-Mesozoic sedimentary piles (Heinisch et al. 1987; Lein et al. 1997).

The Jenig Complex is situated at the northern slopes of the Gail valley within an about 100 km long and up to 15 km wide belt (Fig. 1B). In Neubauer et al. (1999) it is referred to as a continuous lithostratigraphic unit termed "Gailtal Crystalline Complex". However, the overlying Permo-Mesozoic sediments do not represent a continuous sedimentary cover, but consist of three parts characterised by different facies evolutions (Lein et al. 1997). At least two of these parts have preserved transgressive contacts to the crystalline basement at the northern slopes of the Gail valley.

The tectonic position of the crystalline basement of the Drau range within the Austroalpine nappe pile was interpreted in different ways over the past decades (Tollmann 1963: "Middle Austroalpine"; Tollmann 1977: "Upper Austroalpine"). In this work we follow the nomenclature by Schmid et al. (2004) where it belongs to the Drauzug-Gurktal nappe system of the Upper Austroalpine unit (Fig. 1B). According to Schmid et al. (2004) the Drauzug-Gurktal nappe system is part of the tectonic upper plate during the eo-Alpine tectonothermal event. For this reason it experienced only a weak eo-Alpine metamorphism and thus the pre-Alpine assemblages are well preserved in areas without eo-Alpine phyllonitization.

First detailed lithological maps covering most of the crystalline basement at the northern slopes of the Gail valley were published by Heritsch and Paulitsch (1958) and Paulitsch (1960). According to these maps the dominant schistosity in the rocks is dipping moderately or steeply towards the North and the lithological composition includes paragneises, mica schists, quarzitic mica schists, quartzites, orthogneisses, amphibolites, "diaphtorithic" rocks and phyllites. Garnet, staurolite and in some case also kyanite-bearing mica schists and paragneisses were found in the westernmost sector up to Liesing and also in a narrow belt along the southern margin between Liesing and Kötschach. In between and towards the East retrograde metamorphic rocks and prograde phyllites partly derived from Paleozoic sediments (Schönlaub, 1979) occur (Fig. 2A). Since the crystalline basement rocks are overlain by unmetamorphosed to anchizonal metamorphic Mesozoic sediments (Rantitsch, 2001), the medium-grade metamorphism in the basement was recognized to be pre-Alpine. Some authors (Purtscheller and Sassi 1975; Bögel et al. 1979) related the medium-grade imprint to a Caledonian (Ordovician) event, because they interpreted gaps between medium- and low-grade basement rocks as masked Caledonian discordances.

Based on results from anew mapping Heinisch (1987) pointed out that the crystalline basement is strongly affected by eo-Alpine and Alpine ductile and brittle deformation, internally and also along the margins, especially along the Periadriatic fault (Heinisch and Spengler 1988). The "diaphthoritic" rocks represent phyllonites, formed at least partly during the eo-Alpine tectonothermal event. Furthermore Heinisch (1987) subdivided the "Gailtalkristallin" into four different zones (Fig. 2B): 1) a zone of garnet-mica schists, 2) a phyllonite zone, 3) a zone with staurolite-garnet mica schists with some occurrences of sillimanite (Heinisch et al. 1983) and 4) a zone of (un)metamorphosed Paleozoic rocks.

These zones are separated by subvertical E-W-trending semiductile and ductile sinistral strike-slip shear zones (Heinisch 1987; Unzog, 1989a, 1989b, 1991, 1992). In the south the units and shear zones are cut by the ESE-WNW orientated Periadriatic fault.

The zone of metamorphosed Paleozoic rocks (Zone 4 of Heinisch et al. 1983) comprises phyllonitic mica schists and phyllites with layers of greenschists, amphibolites, quartzites, black graphitic schists and even marbles. From one of these marbles Paleozoic (probably Silurian) conodonts have been reported (Schönlaub, 1979). Whereas the main part of this zone shows a greenschist-facies imprint, in a restricted area north of Jenig, Heinisch (1987) discovered nicely preserved staurolite together with garnet in the surrounding. Based on these observations he interpreted the metamorphic history of the "Gailtal crystalline basement" as follows: during the Variscan tectonothermal event zones 1-3 experienced amphibolite-facies conditions, whereas in zone 4 only greenschist-facies

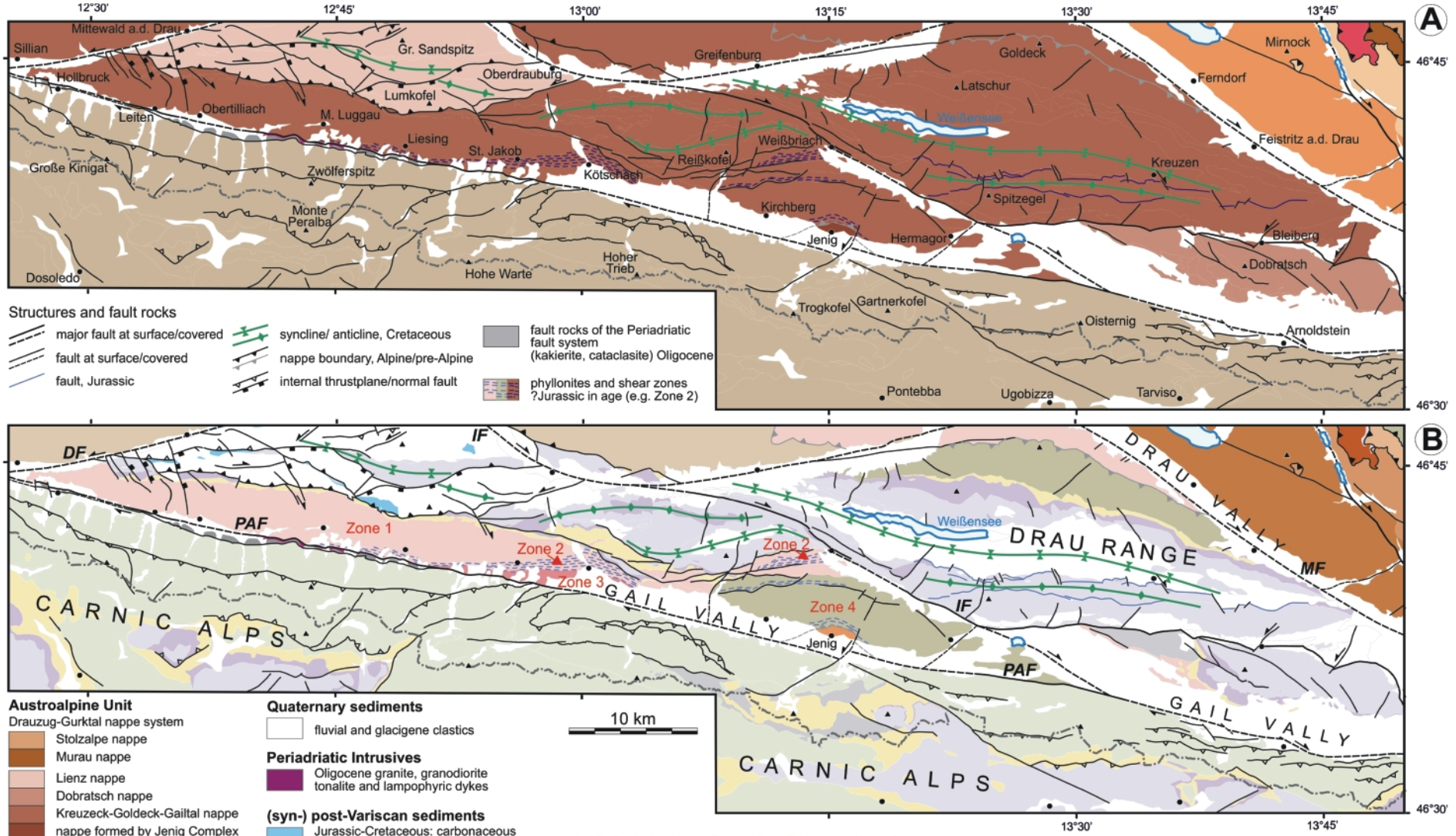
12°30'
12°45'
13°00'
13°15'
13°30'
13°45'
A
B
46°45'
46°30'
Mittewald a.d. Drau
Sillian
Hollbruck
Leiten
Obertilliach
Gr. Sandspitz
Oberdrauburg
Lumkofel
M. Luggau
Liesing
St. Jakob
Große Kinigat
Zwölferspitz
Monte Peralba
Dosoledo
Hohe Warte
Hoher Trieb
Kötschach
Greifenburg
Reißkofel
Weißbriach
Kirchberg
Jenig
Hermagor
Trogkofel
Gartnerkofel
Pontebba
Ugobizza
Tarviso
Oisternig
Goldeck
Latschur
Weißensee
Spitzegel
Kreuzen
Ferndorf
Mirnock
Feistritz a.d. Drau
Bleiberg
Dobratsch
Arnoldstein
Structures and fault rocks
major fault at surface/covered
fault at surface/covered
fault, Jurassic
syncline/ anticline, Cretaceous
nappe boundary, Alpine/pre-Alpine
internal thrustplane/normal fault
fault rocks of the Periadriatic fault system (kakierite, cataclasite) Oligocene
phyllonites and shear zones ?Jurassic in age (e.g. Zone 2)
DF
IF
PAF
MF
Zone 1
Zone 2
Zone 3
Zone 4
CARNIC ALPS
GAIL VALLY
DRAU VALLY
DRAU RANGE
10 km
Austroalpine Unit
Drauzug-Gurktal nappe system
Stolzalpe nappe
Murau nappe
Lienz nappe
Dobratsch nappe
Kreuzeck-Goldeck-Gailtal nappe
nappe formed by Jenig Complex
Ötztal-Bundschuh nappe system
Bundschuh nappe
Koralpe-Wölz Nappe system
Gstoder nappe (formed by Radenthein Complex)
nappe formed by Millstatt Complex
Southalpine Unit
unsubdivided
Quaternary sediments
fluvial and glacigene clastics
Periadriatic Intrusives
Oligocene granite, granodiorite tonalite and lampophyric dykes
(syn-) post-Variscan sediments
Jurassic-Cretaceous: carbonaceous and siliciclastic basinal sediments
Norium-Rhaethium: platform carbonates
Ladinium-Karnium: plattform carbonates with terrigenous material
Anisium: shallow basinal limestones
Permian-Lower Triassic: fluviatil, shallow marine sediments and volcanics
Carboniferous: flyschoid and fluvial clastic sediments
pre-Variscan metasediments and magmatic rocks
Ordovician-Devonian, limestone, marble, dolomite, schist
Variscan and Eoalpine diagenesis to anchizone
Ordovician-Devonian, phyllite, marble, greenschist
Variscan lower greenschist-facies (e.g Zone 4, Goldeck Complex)
Ordovician-Devonian, phyllite, garnet-mica schist, amphibolite
Variscan greenschist-facies (e.g. Turntal Complex)
Neoproterozoic-Devon, garnet-mica schist, paragneiss, orthogneiss
Variscan upper greenschist to amphibolite-facies (e.g. Zone 1)
Neoproterozoic-Devon, staurolite-garnet-mica schist, orthogneis
Variscan amphibolite-facies (e.g. Zone 3)
Ordovizium-Silurian, andalusite-staurolite-garnet-mica schist paragneiss
Permian low pressure amphibolite-facies (Jenig Complex)
Ordovizium - Devonian; (garnet)-mica schist, amphibolite
Eoalpine upper greenschist-facies
Neoproterozoic - Ordovizian; paragneiss, amphibolite, orthogneiss
Variscan and Eoalpine greenschist to amphibolite-facies
Ordovizium - Devon; garnet-mica schist, amphibolite, marble, quartzite
Eoalpine epidote amphibolite-facies; Radenthein Complex
Neoproterozoic - Devonian; paragneiss, pegmatite gneiss, amphibolite
Eoalpine amphibolite to eclogite-facies; Millstatt Complex

assemblages developed. The eo-Alpine event is responsible for a metamorphic overprint and phyllonitization especially in zone 2. It reached lower greenschist-facies condition except in a part of zone 4 where amphibolite-facies conditions occur in a "metamorphic dome" north of Jenig. Unfortunately Heinisch (1987) lacked geochronological data to prove his model.

Some years later Philippitsch et al. (1986) investigated the gorge North of Jenig and additionally to garnet and staurolite they found andalusite within the metapelites. Furthermore veins composed of andalusite and quartz along with some staurolite and kyanite were discovered. Based on the occurrence of these index minerals they deduced P-T conditions of c. 530 °C at less than 0.5 GPa. They speculated about an Oligocene age of the low-pressure imprint which should be related to an unknown magmatic body of the Periadriatic magmatic suite in the subsurface.

First Ar-Ar and Rb-Sr age determinations from the andalusite-bearing rocks from the gorge to the North of Jenig published by Schuster et al. (2001) yielded Late Triassic to Early Jurassic ages. This data clearly argue against Oligocene contact metamorphism or eo-Alpine (Cretaceous) regional metamorphism. However, they also do not reflect cooling of the rocks after the peak of the Variscan P-T-t loop, because typical Variscan cooling ages are in the range of 290-320 Ma. Therefore, and with respect to regional considerations, Schuster et al. (2001) interpreted these data as cooling ages after a distinct Permo-Triassic HT/LP metamorphic event. However, the existing data might also be interpreted as Variscan cooling ages partly reset during the eo-Alpine event or even as indications for a possible Jurassic thermal overprint.

Neubauer and Genser (2009) determined Ar-Ar muscovite ages of about 315 Ma in the zone of mica schists and 310–312 Ma in the northern part of the phyllonite zone. These data prove cooling of these units in a late stage of the Variscan tectonometamorphic event. In the southern part of the phyllonite zone, close to the staurolite-garnet mica schists they determined Early Jurassic ages of about 180 Ma and therefore they interpreted this part as a Jurassic shear zone. Furthermore they argue that the Ar-Ar spectra show only a weak indication for a Cretaceous eo-Alpine thermal overprint.

To unravel the metamorphic history of the Jenig Complex it was necessary to date the garnet and staurolite-bearing assemblage. Based on the knowledge of the *P-T-t* evolution of the Jenig Complex and its relationship to other parts of the crystalline basement at the northern slopes of the Gail valley the knowledge about the internal structure can be significantly improved which was the impetus of this study.

**Figure 2:** Geological map covering the crystalline basement at the northern slopes of the Gail valley between Hollbruck and Arnoldstein (Carinthia, Austria) and surrounding areas. Map compiled from map sheets GKÖ196-200 of the Austrian Geological Survey (Anderle, 1977; Schönlaub, 1985, 1987, 1989, 1997, 2000), Carta geologica d'Italia Interattiva 1:100000 map sheets 4c-13, 14 and 14a (Amanti et al. 2002), Heinisch (1987) and Probst et al. (2003). (A) Tectonic map based on nomenclature by Schmid et al. (2004) and subdivision of the Drau Range by Lein et al. (1997). Explanation see first column of lower legend. (B) Chronostratigraphic and lithological map. Explanation see column two, three and four of lower legend. Zone 1-4 refers to nomenclature by Heinisch (1987). The dominant metamorphic imprint in the pre-Variscan metasediments and magmatic rocks is highlighted. Major faults with nomenclature partly based on Probst et al. (2003): PAF…Periadriatic fault, DF…Drau fault, IF…Isel fault, MF…Mölltal fault.

## 3. Analytical methods

### 3.1 Whole rock and mineral chemistry

Whole rock and mineral chemical data were measured at the Institute of Mineralogy and Petrography at the University of Innsbruck. Major and trace elements of metapelitic rocks were determined on glass beads and powder pellets by wavelength-dispersive X-ray fluorescence (WDXRF). A JEOL 8100 SUPERPROBE electron microprobe was used for analysing the mineral compositions. Analytical conditions were 15 kV acceleration voltage and 10 nA beam current. Natural and synthetic mineral standards were used for calibration. The counting times were 20 sec. for the peak and 10 sec. for the background. Mineral formulae were calculated using the program NORM (Ulmer, 1993, written comm.).

### 3.2 Rb-Sr and Sm-Nd method

Mechanical and chemical separation for the Sm-Nd and Rb-Sr isotope analyses were performed at the Geological Survey of Austria (Geologische Bundesanstalt) in Vienna. Minerals were separated by standard methods of crushing, grinding, sieving and magnetic separations. Garnet separates were hand-picked under the binocular microscope from defined sieve (0.20-0.30 mm) and magnetic fractions. To remove surface contaminants all mineral fractions were washed in acetone and water before decomposition and leached in 2.5 N HCl at ca. 80 °C for c. 30 minutes. Weights of samples used for dissolution were about 100 mg for whole rock powder, 30–150 mg for garnet and staurolite and about 200 mg for biotite. The chemical sample preparation follows the procedure described by Sölva et al. (2005). Element concentrations were determined by isotope dilution using mixed Sm-Nd and Rb-Sr spikes. Overall blank contributions were <0.3 ng for Nd and Sm and <1 ng for Rb and Sr. Isotopic measurements were done at the Department of Lithospheric Research at the University of Vienna. Spiked Sr and Rb ratios were measured at a MICROMAS M30 machine, spiked Sm, Nd ratios on a Finnigan® MAT 262 MC-TIMS, whereas unspiked Nd ratios were analysed at a ThermoFinnigan® Triton MC-TIMS. All elements were run from Re double filaments, except Rb which was evaporated from a Ta-filament. On the Triton MC-TIMS the La Jolla standard yielded $^{143}Nd/^{144}Nd = 0.511843\pm2$ (n = 13; 2σ standard deviation) whereas for the NBS987 standard a ratio of $^{87}Sr/^{86}Sr = 0.71013\pm4$ (n = 6; 2σ standard deviation) was determined at the MICROMAS M30. Errors for the $^{147}Sm/^{144}Nd$ and $^{87}Rb/^{86}Sr$ ratio are <1%, based on iterative sample analysis and spike recalibration. Ages were calculated with the software ISOPLOT/Ex (Ludwig, 2003). Ages are based on decay constants of $1.393 \times 10^{-11}$ $a^{-1}$ for $^{87}Rb$ (Nebel et al. 2011)

and 6.54 x $10^{-12}$ $a^{-1}$ for $^{147}Sm$.

### 3.3 Monazite dating using the EMS-technique

Monazite and xenotime chemical analyses were performed on a JEOL JX 8600 microprobe following the routine established at the Abteilung Mineralogie, Universität Salzburg. The routine involves a complete wavelength dispersive (WD) analysis for elements Si, P, La, Ce, Pr, Nd, Sm, Gd, Dy, Er, Yb, Y, Th, U, Ca and Pb. A detailed description of standards, element lines, counting times, background positions, background, and interference corrections used in the Salzburg microprobe laboratory for monazite and xenotime analysis is given in Krenn et al. (2008). Chemical Th-U-Pb ages for monazite were calculated following the method of Montel et al. (1996) (Table 9). The analytical errors of a point analysis typically correspond to a ~10-30 Ma error on the age (1 σ). A weighted average age with reduced error can be calculated from a larger number of measurements in coherent age domains.

## 4. Field relations and lithological descriptions

Outcrops of the Jenig Complex located directly to the North of the village Jenig cover an area which extends about 500 m towards the north and can be followed over 3 km along the northern slopes of the Gail valley. To the south the Jenig Complex is covered by Quaternary sediments, but most probably continues in the subsurface until the Periadriatic fault, which is running along the southern margin of the valley. To the North it is separated from phyllonitic mica schists and prograde metamorphic phyllites by a several hundred meters wide pre-Alpine phyllonite zone (Heinisch 1987). The best outcrops of the Jenig Complex can be found in the gorge north of the village Jenig (Philippitsch et al. 1986, Fig. 3) and along the road from Jenig to Kreuth.

The Jenig Complex consists of mica schists, quarzitic mica schists and paragneisses which are partly rich in graphite. Intercalations of up to a few meters thick garnet- and hornblende-bearing quartzites are scarce. In the river bed near to the bridge andalusite-bearing quartz veins are present. Recently the outcrop conditions are bad but these veins were described in detail by Philippitsch et al. (1986).

In the field the mica schists and paragneisses of the Jenig Complex can be distinguished from the overlying phyllonitic mica schists and phyllites also by their structural imprint. The latter are thin-bedded and characterised by frequent chevon-type folds and conjugate kinks. Quartz mobilisate segregations mostly form irregular pods and rods. On the other hand the paragneisses and mica schists of the Jenig Complex form layered outcrops with concordant quartz-plagioclase mobilisate layers, which can be traced over distances of several meters. During the predominant deformational event ($D_x$) these moblisate layers were isoclinally folded and the axial plane cleavage $S_x$ dips towards NNW–NE with about 50° to 65°. The fold axes $F_x$ scatter but generally dip towards the North, parallel to a weakly developed stretching lineation ($L_x$). An overprinting event ($D_{x+1}$) causes open folding by NE-SW orientated axes and a contemporaneous crenulation.

The mica schists of the Jenig Complex are fine-grained and they are composed of muscovite + biotite + chlorite + quartz. They include mineral-rich layers containing garnet, staurolite and andalusite. The metamorphic history of the Jenig Complex can be determined best by these mineral-rich mica schists.

| Sample | RS11/98 | RS13/98 | | RS11/98 | RS13/98 |
|---|---|---|---|---|---|
| | [wt%] | | | [ppm] | |
| $SiO_2$ | 44.39 | 49.34 | As | < 1 | 3 |
| $TiO_2$ | 1.17 | 1.43 | Ba | 872 | 766 |
| $Al_2O_3$ | 26.49 | 23.78 | Ce | 95 | 112 |
| $Fe_2O_3$ | 12.06 | 12.14 | Cl | < 20 | < 20 |
| FeO | 10.85 | 10.92 | Co | 30 | 35 |
| MnO | 0.11 | 0.25 | Cr | 149 | 174 |
| MgO | 3.33 | 2.72 | Cs | 12 | 7 |
| CaO | 0.71 | 0.54 | Cu | 118 | 39 |
| $Na_2O$ | 1.52 | 1.29 | F | 560 | 320 |
| $K_2O$ | 6.11 | 4.31 | Ga | 43 | 34 |
| $P_2O_5$ | 0.38 | 0.24 | La | 73 | 81 |
| C | 0.34 | 0.64 | Mo | < 1 | < 1 |
| $CO_2$ | | | Nb | 25 | 27 |
| $H_2O$ | 3.73 | 3.36 | Nd | 59 | 68 |
| **Total** | **100.34** | **100.04** | Ni | 60 | 66 |
| | | | Pb | 38 | 27 |
| Total $Fe_2O_3$ | 100.34 | 100.04 | Pr | 18 | 18 |
| Total FeO | 99.13 | 98.82 | Rb | 233 | 144 |
| X Mg | 0.23 | 0.20 | S | 90 | 450 |
| | | | Sc | 25 | 24 |
| | | | Sm | 13 | 14 |
| | | | Sn | 6 | 5 |
| | | | Sr | 231 | 211 |
| | | | Th | 17 | 19 |
| | | | U | 4 | 4 |
| | | | V | 235 | 195 |
| | | | Y | 50 | 59 |
| | | | Zn | 233 | 154 |
| | | | Zr | 178 | 286 |

**Table 1:** Whole rock geochemistry of Al-rich metapelites: With respect to the average pelite from Symmes and Ferry (1991) the mica schists of the Jenig Complex are enriched in $Al_2O_3$, $Fe_2O_3$, $K_2O$ and depleted in $SiO_2$, CaO and $Na_2O$.

**Figure 3:** Petography of the Al-rich metapelites of the Jenig Complex: (A) fine-grained matrix composed of white mica + chlorite + quartz + biotite + ilmenite + graphite is overgrown by garnet and bioite porphyroblasts (RS37/00, parallel polarized); (B) the succession of porphyroblast growth is garnet + biotite followed by staurolite + biotite and andalusite + biotite (RS9/98, parallel polarized); (C, D) Staurolite within andalusite shows a core with fine-grained graphitic pigment and a rim with myrmecitic intergrowths of staurolite + quartz (RS37/00, parallel polarized); (E) Staurolite and andalusite overgrowing a fine-grained white mica rich matrix. Within and at the boundaries of andalusite cleavage domes with graphite are present (RS37/00, parallel polarized). (F) Quartzite with a matrix of quartz and plagioclase, overgrown by garnet and amphibole poikiloblasts (JEN-14/2, parallel polarized). (G) Andalusite-bearing quartz vein with idiomorphic andalusite crystals and some tourmaline (JEN-14/2, parallel polarized). (H) Andalusite-bearing quartz vein with kyanite growing at the boundary between two andalusite crystals (JEN-3A, parallel polarized).

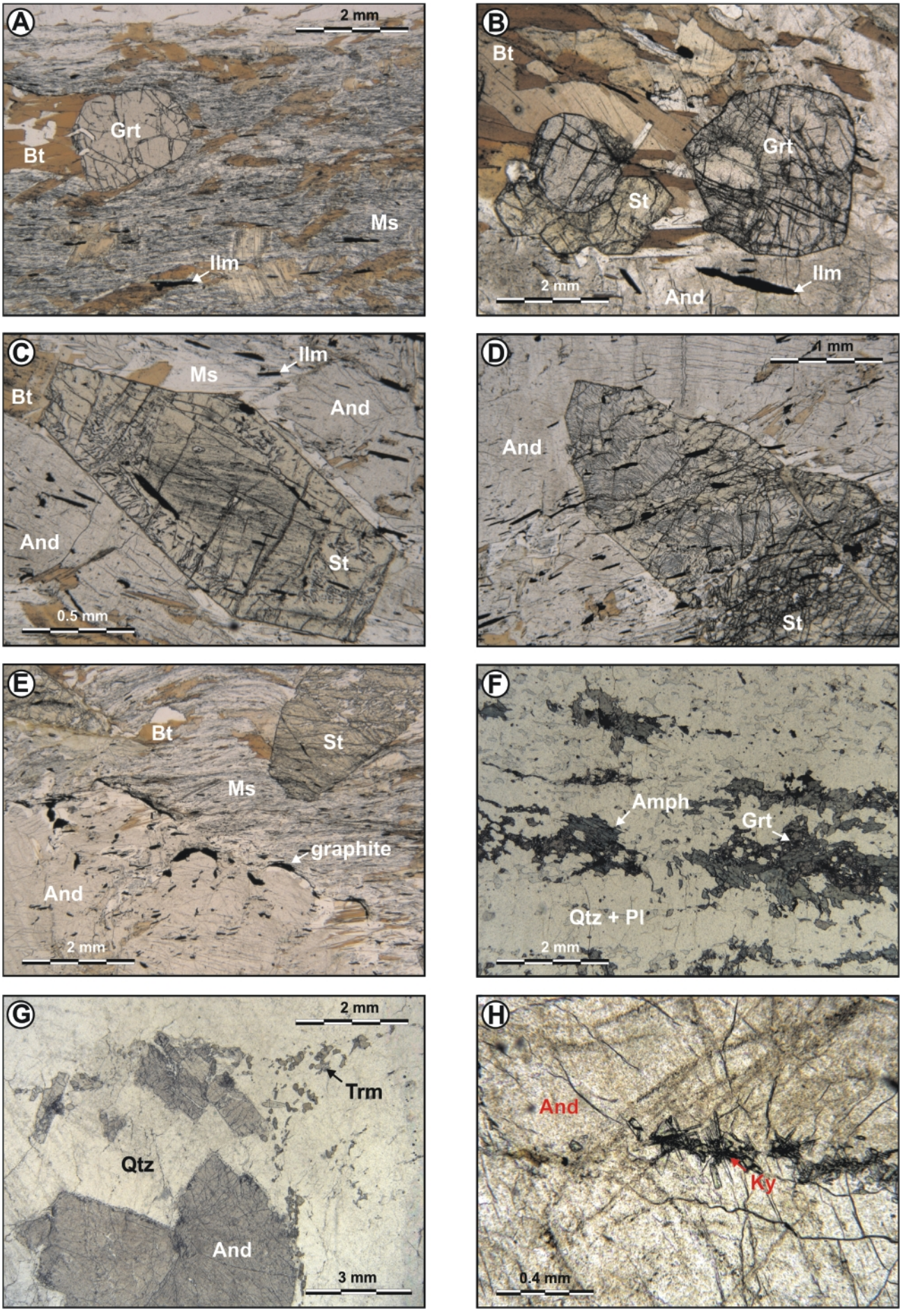
A
2 mm
Grt
Bt
Ms
Ilm
B
Bt
Grt
St
Ilm
2 mm
And
C
Ilm
Ms
Bt
And
And
St
0.5 mm
D
1 mm
And
St
E
Bt
St
Ms
graphite
And
2 mm
F
Amph
Grt
Qtz + Pl
2 mm
G
2 mm
Trm
Qtz
And
3 mm
H
And
Ky
0.4 mm

With respect to the "average" pelite from Symmes and Ferry (1991) they are enriched in $Al_2O_3$, $Fe_2O_3$, $K_2O$ and depleted in $SiO_2$, CaO and $Na_2O$ and developed from shales according to the diagram of Garia et al. (1991) (Table 1).

## 5. Petrography

In this chapter the lithologies of the Jenig Complex are described. Samples were collected from the eastern side of the gorge entering the northern slopes of the Gail valley north of Jenig (WGS84 N 46°37'51''/E 013°15'14'').

### 5.1 Al-rich metapelites

The samples of Al-rich metapelites are characterised by mineral assemblages including staurolite, garnet, andalusite, biotite, muscovite, plagioclase, quartz, chlorite, ilmenite, graphite, clinozoisite, monazite, apatite, zircon and tourmaline. The matrix consists of fine-grained muscovite + biotite + chlorite + quartz and contains garnet and staurolite (up to 15 mm large) porphyroblasts as well as millimetre-sized biotite flakes which overgrow the dominant schistosity ($S_x$). In some layers andalusite overgrows the older textures. Andalusite is barely visible in hand specimen, but it occurs in graphite-rich lithologies together with coarse-grained biotite flakes.

In thin sections the oldest visible schistosity ($S_{x-1}$) is preserved within cleavage domains of the dominating schistosity ($S_x$). Quartz-plagioclase mobilisate layers are partly orientated parallel to $S_{x-1}$ and isoclinally folded by $S_x$. $S_{x-1}$ as well as $S_x$ and are defined by fine-grained textures composed of white $mica_1$, quartz and minor $chlorite_1$, $biotite_1$, ilmenite and $plagioclase_1$. The textures also show dispersed graphitic pigment (Fig. 3A). This texture is overgrown by $biotite_2$, followed by garnet + $biotite_2$ and again followed by staurolite + $plagioclase_2$. The youngest porphyroblasts are andalusite crystals, which grow together with coarse-grained $biotite_2$ and white $mica_2$ (Fig. 3B). Also coarse-grained plagioclase and $chlorite_2$ are present in the andalusit-bearing domains. All porphyroblasts overgrowing the $S_x$ textures are more or less orientated within a stretching lineation $L_{x+1}$. They are undeformed except for white $mica_2$ and $biotite_2$, which are unduloese and kinked in some places. In the matrix a weak deformation $D_{x+1}$ is visible by locally developed open folds in the vicinity of the porphyroblasts. Sometimes also a crenulation ($F_{x+1}$) with fold axes orientated parallel to $L_{x+1}$ is present. As the geometry of the kinkbands of $biotit_2$ shows the same shear sense as the deformation $D_x$ and $D_{x+1}$ seem to be stages in a continuous process. In some samples pure shear outlasts the growth of all prophyroblasts, because in these samples the coarse-grained micas show a weak preferred orientation and even the andalusite is slightly unduloese. In one sample andalusite grows perpendicular to the foliation $S_x$. Most probably it grew in an extensional environment with σ1 parallel to the stretching lineation $L_{x+1}$. During cooling of the rocks through the brittle-ductile transition, distinct fractures filled with quartz, albite and $chlorite_3$ formed during deformation stage $D_{x+2}$. In some samples these fractures form a conjugate system. Along the fractures sericitization and chloritization can be observed.

*Garnet* normally reaches 0.5-2 mm in diameter but sometimes porphyroblasts up to 4 mm are present. In general they are idiomorphic and contain only very few inclusions of quartz and ilmenite, especially in the outer parts. In sample RS10/98 the cores of the garnets are poikiloblastic and contain fine-grained quartz and graphitic pigment. Theses inclusions indicate a fine-grained, planar texture of the matrix during the growth of the garnet cores. In some samples garnet forms elongated aggregates within the stretching lineation $L_{x+1}$. Sometimes the cores are broken and the pieces drifted away from each other. Rarely garnet crystals with minor chloritization along the edges have been observed.

*Staurolite* forms up to 15 mm large, idiomorphic porphyroblasts statically overgrowing the schistosity $S_x$. It is often present in direct contact with garnet. As inclusions graphitic pigment, quartz, ilmenite and idiomorphic garnet crystals occur. Staurolite crystals which are overgrown by andalusite frequently show an idiomorphic, graphite-rich core and a graphite-poor rim (RS13/98). In several cases these rims show fine-grained myrmekitic textures composed of staurolite and quartz (Fig. 3C, D). In sample RS7/98 tiny idiomorphic staurolite grains occur at the contact to andalusite.

*Biotite* is present as small flakes orientated in the foliation ($S_{x-1}$ and $S_x$) of the matrix ($biotite_1$) and as coarse-grained porphyroblasts ($biotite_2$) overgrowing the foliation. $Biotite_2$ porphyroblasts are sometimes kinked and show unduloese extinction.

*Muscovite* is a main constitute of the matrix ($muscovite_1$) where it is present as fine-grained flakes orientated in $S_{x-1}$ and $S_x$. Coarse-grained $muscovite_2$ is present in the vicinity of andalusite and as inclusions within andalusite.

*Quartz* is also a main constitute of the matrix and forms mobilisate layers. Within the latter it is coarse-grained, and dynamically recrystallized with bulging and subgrain rotation.

*Plagioclase* forms fine-grained aggregates with triple junctions within the matrix, and especially in cleavage domains of $S_x$. In the vicinity of staurolite porphyroblasts large plagioclase crystals overgrow the fine-grained matrix.

*Andalusite* is present as up to a few centimetre large poikiloblatic crystals, partly showing idiomorphic edges. In some cases andalusite displaces graphitic pigment which is enriched in cleavage domes (Fig. 3E). These cleavage domes are later overgrown in several stages. In one sample the overgrown graphitic pigment indicates, andalusite growth within a fine-grained matrix with some coarse-grained white mica flakes not orientated in $S_x$. Around the andalusite phorphyroblasts the growth of coarse-grained $biotite_2$ and $muscovite_2$ can be observed. Andalusite overgrows garnet, staurolite, $biotite_2$ and also some $muscovite_2$, whereby the micas are partly resorbed. In some cases andalusite has been replaced by coarse-grained $muscovite_3$ and $biotite_2$. Chlorite flakes within andalusite observed in one sample represent pseudomorphs after $biotite_{1\ or\ 2}$, because they exhibit rutile exolutions. The chlorite is a late stage product, which formed contemporaneously with sericitization of andalusite, starting along cracks.

*Ilmenite* is present as up to 1 mm large crystals orientated in $S_{x-1}$ and $S_x$ respectively.

*Clinozoisite* has been found within quartz mobilisate layers.

### 5.2 Quartzite

The quarzites show a fine-grained matrix of quartz and minor plagioclase, which are overgrown by poikiloblastic amphibole and garnet (Fig. 3F). In addition epidote and opaque ore is present. Quartz shows just a weak shape-preferred orientation, grain boundary migration and intense unduloese extinction. Plagioclase is characterised by polysynthetic twinning and a somewhat smaller grain size with respect to quartz. The garnet and amphibole poikiloblasts are often strongly elongated within the schistosity.

### 5.3 Andalusite-bearing quartz veins

The andalusite-bearing quartz veins have been described in detail by Philippitsch et al. (1986). They are more or less concordant within the main foliation $S_x$ but show an irregular shape. Andalusite crystals are up to 10 cm in length and occur at the margins but also in the centre of the vein. They are irregularly distributed within a quartz matrix and show no preferred orientation. The crystals are prismatic (Fig. 3G) and pinkish to greyish coloured. In some cases their surfaces are covered with muscovite. In thin sections scarce kyanite needles, growing within and along the edges of the andalusite are visible (Fig. 3H). In one sample (JEN-3) idiomorphic staurolite crystals up to some millimetres in size occur along grain boundaries of large andalusite crystals. Another sample from the margin of a vein (JEN-6) contains tourmaline as inclusions in andalusite and quartz. Tourmaline with the same brownish green colour is also frequently observed in the metapelitic wall rock. Furthermore some plagioclase and aggregates of coarse-grained (>5 mm) bended muscovite is present. A slight ductile deformation is responsible for the irregular lense-shape of the veins, plastic deformation and semi-ductile bending of some of the andalusite crystals and undulosity of quartz.

This andalusite-bearing quartz veins are interpreted to represent mobilisates from the surrounding Al-rich-metapelites.

## 6. Mineral chemistry

*Garnet:* The chemical composition of garnet is very similar

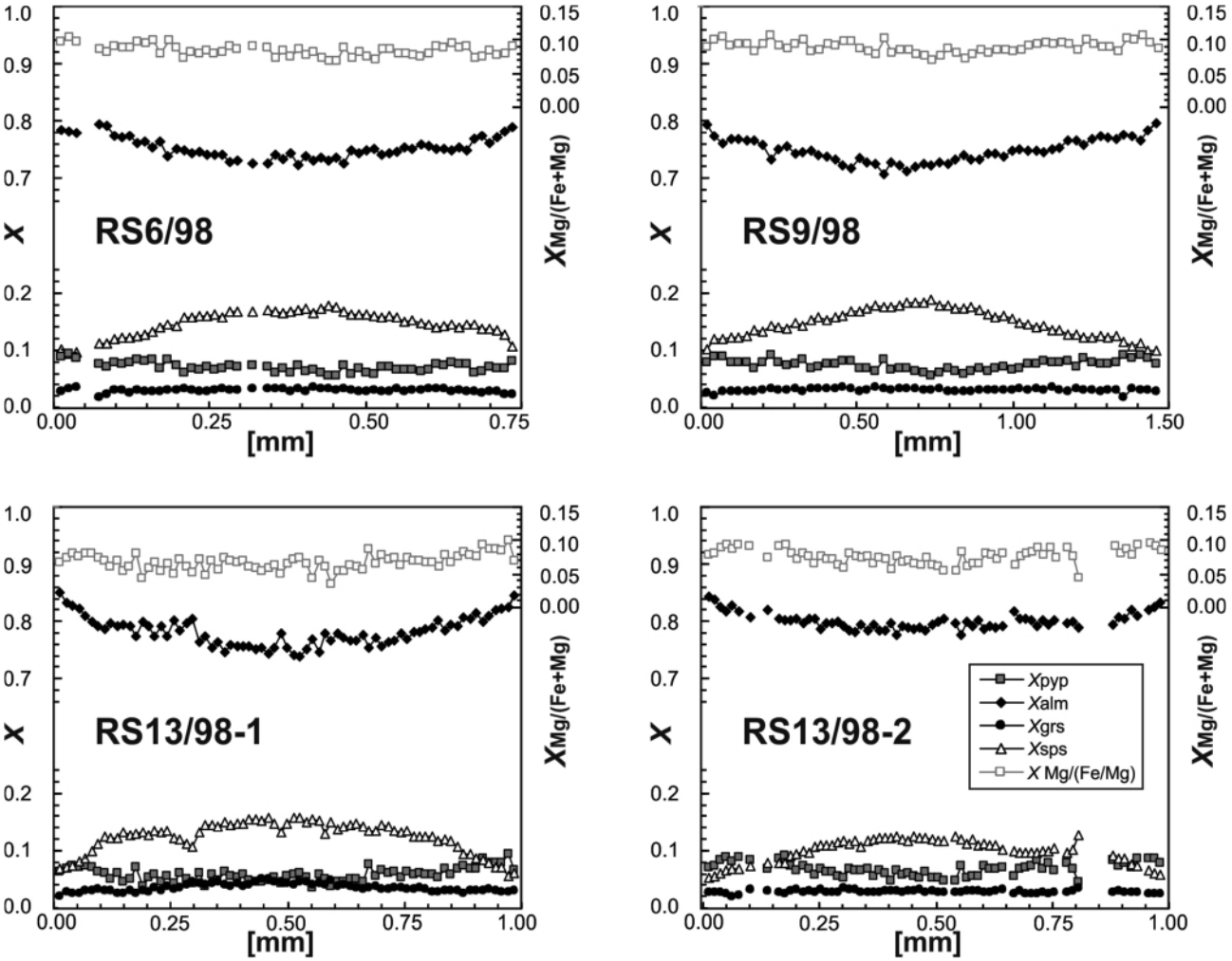


**Figure 4:** Chemical composition of garnets from the Jenig Complex: The composition of all investigated crystals is very similar. In general they are rich in almandine and display growth zoning characterised by a shallow increase of *X*alm and *X*prp from the centre towards the rim, which is compensated by an inverse zoning of *X*sps. *X*grs is low and shows no variation.

in the three investigated samples (Fig. 4). In general it is rich in almandine and display growth zoning characterised by a shallow increase of *X*alm and *X*prp from the centre towards the rim, which is compensated by an inverse zoning of *X*sps. As *X*alm and *X*pyp show the same trend the Mg number [Mg/(Fe$^{2+}$+Mg)] is more or less constant and in the range of 0.05-0.13. *X*grs shows no variation. In the cores Mn reaches up to 0.55 atoms per formula unit (a.p.f.u) which corresponds to almost *X*sps = 0.2. The garnet rim compositions are relatively homogeneous with *X*alm = 0.76–0.83, a significant *X*sps component (0.07–0.14) and low Xpyp (0.07–0.08) and *X*grs (0.02–0.03) components.

*Staurolite:* All staurolites are rich in Fe$^{2+}$ and the Fe number [Fe$^{2+}$/(Fe$^{2+}$+Mg)] varies between 0.85 and 0.92. Some crystals show a continuous chemical zoning with slightly decreasing MgO and ZnO contents and an increasing Fe number towards the margins. Also rims with significant MnO and ZnO contents of 0.2–0.4 and 0.9–3.0 wt.% respectively have been observed.

*Plagioclase* ($An_{13-19}$) is chemically homogeneous throughout the investigated samples.

Biotite: All biotites are unzoned and rich in FeO (19–22 wt.%). $TiO_2$ is low and varies between 1.47 and 1.88 wt.%.

*Muscovite* shows Si contents of 3.05–3.07 Si a.p.f.u. and relatively high paragonite contents of 24–27 mol.%.

Selected mineral analyses are shown in Table 2.

| Sample | RS 9/98 | RS 9/98 | RS 9/98 | RS 9/98 |
|---|---|---|---|---|
| Mineral | Grt | Bt | Pl | Ms |
| $SiO_2$ | 37.90 | 36.08 | 64.76 | 46.55 |
| $TiO_2$ | 0.01 | 1.51 | 0.01 | 0.25 |
| $Al_2O_3$ | 21.51 | 19.92 | 22.29 | 37.13 |
| $Fe_2O_3$ | n.c. | n.c. | 0.48 | n.c. |
| FeO | 36.53 | 21.42 | n.d. | 0.97 |
| MnO | 2.89 | 0.12 | 0.01 | 0.03 |
| MgO | 1.96 | 8.17 | 0.02 | 0.27 |
| CaO | 0.84 | n.d. | 3.03 | n.d. |
| $Na_2O$ | n.d. | 0.25 | 9.95 | 2.15 |
| $K_2O$ | n.d. | 9.15 | 0.08 | 8.43 |
| [wt%] Σ | **101.64** | **96.63** | **100.63** | **95.79** |
| Si | 3.018 | 2.720 | 2.839 | 3.051 |
| Ti | 0.001 | 0.086 | 0.000 | 0.012 |
| Al | 2.020 | 1.770 | 1.152 | 2.869 |
| Fe3+ | n.c. | n.c. | 0.016 | n.c. |
| Fe2+ | 2.433 | 1.350 | n.d. | 0.053 |
| Mn | 0.195 | 0.008 | n.d. | 0.002 |
| Mg | 0.233 | 0.918 | 0.001 | 0.026 |
| Ca | 0.072 | n.d. | 0.142 | n.d. |
| Na | n.d. | 0.037 | 0.846 | 0.273 |
| K | n.d. | 0.881 | 0.004 | 0.706 |
| Σ | **7.971** | **7.768** | **5.002** | **6.992** |

**Table 2:** Representative electron microprobe analysis of minerals used in thermobarometry. Basis of formula calculation: 12 O and 8 cations (garnet), 11 O (muscovite, biotite), 8 O (plagioclase); n.d. not detected; n.c.: not calculated.

## 7. Geothermobarometry

*Multi-equilibrium geothermobarometry:* The simultaneous calculation of all possible reactions within a defined chemical system has been done by using the program THERMOCALC v. 3.21 (Powell and Holland, 2003) and the data set of Holland and Powell (1998). The natural composition of coexisting minerals is taken into account using the activity models for garnet, plagioclase, muscovite and biotite from the set of proposed activity models from the program MacAX (Holland, 2000, written comm.). To avoid uncertainties due to poor knowledge of $H_2O$ activity, only $H_2O$-absent reactions were used. The activities were calculated with starting *P-T* values of 0.6 GPa and 500°C, to determine the *P-T* conditions of the intersections. Subsequently the obtained P-T conditions were then used to re-calculate the activities again. This iteration process was repeated until the data converged to less than 0.01 GPa and 10 °C. For samples containing the assemblage garnet + andalusite + biotite + plagioclase + muscovite + quartz the following reactions, intersecting in two $H_2O$-absent intersections (I, II), were used:

The first invariant point (I) is constrained with the reactions:

$$3CaAl_2Si_2O_8 = Ca_3Al_2Si_3O_{12} + 2Al_2SiO_5 + SiO_2 \quad (1)$$
anorthite = grossular + andalusite + quartz

$$Mg_3Al_2Si_3O_{12} + KAl_2Si_3AlO_{10}(OH)_2 = 2Al_2SiO_5 + KMg_3Si_3AlO_{10}(OH)_2 + 3CaAl_2Si_2O_8 \quad (2)$$
pyrope + muscovite = andalusite + phlogopite + quartz

$$Mg_3Al_2Si_3O_{12} + Ca_3Al_2Si_3O_{12} + KAl_2Si_3AlO_{10}(OH)_2 = KMg_3Si_3AlO_{10}(OH)_2 + 3CaAl_2Si_2O_8 \quad (3)$$
pyrope + grossular + muscovite = phlogopite + anorthite

The second invariant point (II) consists of reaction (3) and the Fe-endmember reaction of (3) and the garnet-biotite exchange equilibrium:

$$Fe_3Al_2Si_3O_{12} + Ca_3Al_2Si_3O_{12} + KAl_2Si_3AlO_{10}(OH)_2 = KFe_3Si_3AlO_{10}(OH)_2 + 3CaAl_2Si_2O_8 \quad (4)$$
almandine + grossular + muscovite = annite + anorthite

$$Fe_3Al_2Si_3O_{12} + KMg_3Si_3AlO_{10}(OH)_2 = Mg_3Al_2Si_3O_{12} + KFe_3Si_3AlO_{10}(OH)_2 \quad (5)$$
almandine + phlogopite = pyrope + annite

Calculations of the *P-T* conditions by using both invariant points in three samples (RS6/98, RS9/98, RS13/98) yielded *P-T* results ranging from 450 to 530°C and 0.24 to 0.42 GPa as shown in Table 3.

| | Intersection I | | | | Intersection II | | | |
|---|---|---|---|---|---|---|---|---|
| Sample | P [GPa] | σ | T [°C] | σ | P [GPa] | σ | T [°C] | σ |
| RS 6/98 | 2.5 | 0.6 | 524 | 46 | 3.7 | 0.6 | 464 | 41 |
| RS 9/98 | 3.7 | 0.7 | 521 | 46 | 4.2 | 0.7 | 495 | 44 |
| RS 13/98 | 2.7 | 0.6 | 514 | 45 | 3.8 | 0.6 | 461 | 41 |

**Table 3:** Results of the multi-equilibrium *P-T* calculations with THERMOCALC v. 3.21.

*Ti-in-geothermobarometry:* Henry et al. (2005) formulated the Ti-in-biotite thermometer for graphitic, peraluminous metapelites that contain graphite, quartz, rutile and/or ilmenite in excess to the mineral assemblage and which equilibrated at pressures of roughly 0.4-0.6 GPa and a temperature range of 480-800°C. The Thermometer is based on the Ti content as well as the ratio of Mg/(Mg + Fe) and was applied to sample RS13/98. The $X_{mg}$ values of biotites are rather constant and c. 0.404, in contrast to the Ti contents, which range from 0.119 to 0.207 a.p.f.u. The resulting temperatures range from 442 to 546°C and agree well with the temperatures from the multi-equilibrium calculations.

## 8. Geochronology

To determine the formation age of the amphibolite-facies assemblage Sm-Nd analyses of garnet and staurolite as well as monazite dating by the EMS-technique were performed.

### 8.1 Sm-Nd method

Sm-Nd analysed were performed on whole rock powders (WR), garnet and staurolite fractions of 4 individual samples Table 4. The whole rocks are characterised by Sm and Nd contents of 8.20–19.1 ppm and 42.7–101 ppm respectively. The corresponding $^{147}Sm/^{144}Nd$ ratios are in the range of 0.106–0.118, εNd values are 14.2–14.8 and the depleted mantle model ages are in a narrow range of 1.59–1.75 Ga. In three of the samples (RS11/98; RS36/00, RS38/00) garnet separates yielded relatively high Nd (5.77–8.24 ppm) and Sm (1.81–2.48 ppm) contents and corresponding low spreads in the $^{147}Sm/^{144}Nd$ ratios (0.1778–0.2174). Therefore no reliable garnet-WR ages can be calculated from these separates. The garnet fraction from sample RS13/97 yielded lower Nd (1.12, ppm) and Sm (0.84 ppm) contents and a higher $^{147}Sm/^{144}Nd$ ratio of 0.452. The calculated age with the WR is 253±7 Ma. Also the analysed staurolite fractions show relatively low Sm (0.57–1.58 ppm) and Nd (1.64–2.70 ppm) contents. The $^{147}Sm/^{144}Nd$ ratio of staurolite from sample RS11/98 is too low for the calculation of a significant age, but the $^{147}Sm/^{144}Nd$ ratios of staurolite fractions of sample RS13/97 are remarkably high (0.353, 0.540). Age calculations with the WR are 231±4 Ma and 244±4 Ma. Plotting all determined data points a linear trend with a calculated age value of 240±14 Ma and an MSWD value of 10.2 can be observed (Fig. 5).

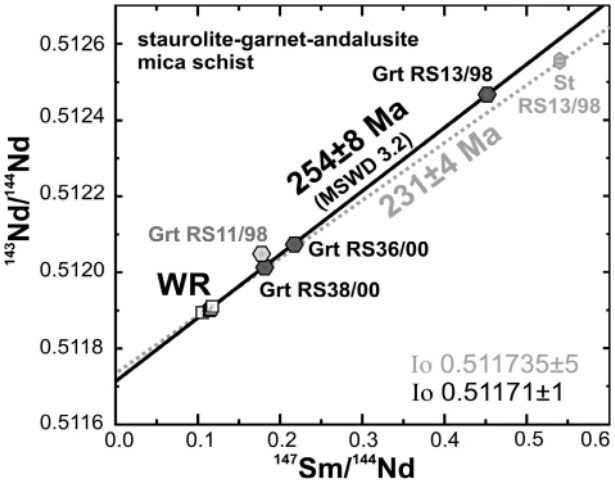


**Figure 5:** Sm-Nd isochron diagram calculated from whole rock, garnet and staurolite analysis. The pooled isochron gives a preferred age value of 254±4 Ma, indicating a late Permian to Early Triassic formation of the amphibolite facies assemblage (for detailed discussion see text).

### 8.2 Rb-Sr dating of biotite

Two Rb-Sr biotite ages from Al-rich metapelites of the Jenig Complex were published by Schuster et al. (2001). Recalculation of the measured data with the decay constant by Nebel et al. (2011) define ages of 178±2 Ma (RS13/98) and 210±22 Ma (RS11/98). An additional age was measured on a sample from zone with staurolite-garnet mica schists west of St. Daniel in the Gail valley (N46°39'53'', E013°05'58''). The rock contains lots of up to 1 cm large idioblastic staurolite porphyroblasts, garnet up to 4 mm and biotite flakes up to 8 mm in diameter within a fine-grained matrix of muscovite and quartz. The age determined for the biotite is 174±2 Ma (RS28/01).

### 8.3 Monazite dating by the EMS-technique

From three individual samples six monazite crystals were measured by the EMS-technique. These monazites form inclusions within all major minerals of the rocks, e.g. staurolite, biotite, and andalusite (Fig. 6). The pooled ages for the individual samples are 278±21 Ma (RS13/98), 272±13 Ma (RS9/98) and 270±21 Ma (RS6/98).

## 9. Discussion

This chapter starts with a discussion on the geological evolution of the Jenig Complex. After that aspects for the definition of the Jenig Complex as a lithodemic unit and nomenclatoric problems with respect to the basement at the northern slopes of the Gail valley will be discussed.

### 9.1 *P-T-t* evolution of the Jenig Complex

#### 9.1.1 Protolith and first metamorphic assemblage

The Jenig Complex comprises relatively homogeneous metapelites and metapsamites of unknown protolith age. The depleted mantle model ages (1.59-1.75 Ga) of the whole rocks fit to those of other Austroalpine units (Thöni, 1999). For these other units Neoproterozoic or early Paleozoic deposition ages are likely and the same can be expected for the protoliths of the Jenig Complex.

The oldest visible metamorphic assemblage in the Al-rich metapelites developed at lower greenschist-facies conditions and includes fine-grained muscovite + biotite + chlorite + quartz. Also the crystallization age of this assemblage is unknown, but it might have formed during the prograde part of the Permian amphibolites facies *P-T-t* loop or during an earlier independent tectonometamorphic event (e.g. the Variscan event).

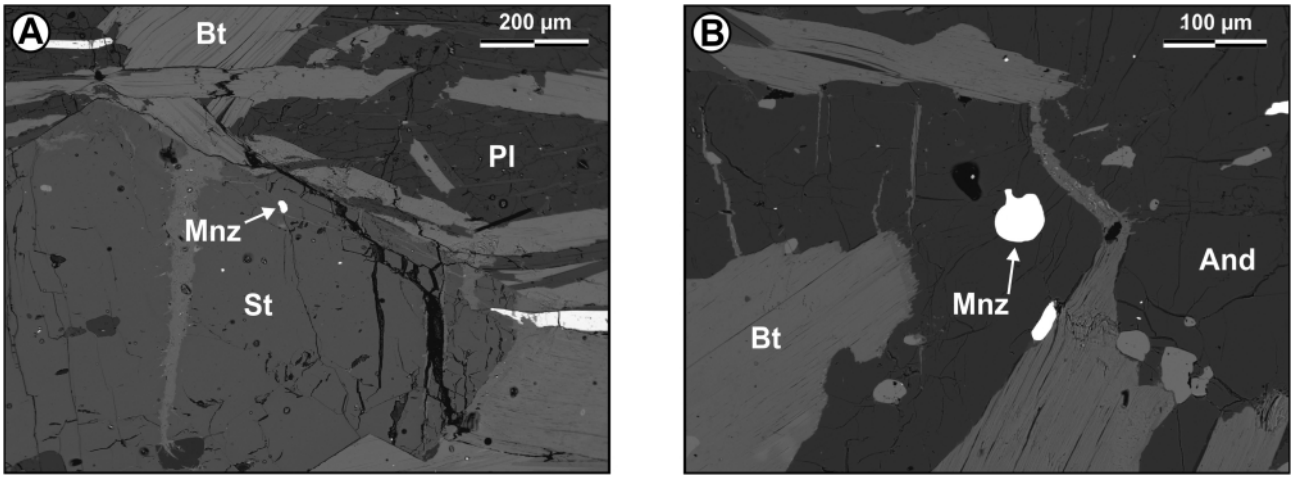


**Figure 6:** Monazite from the Al-rich metapelites of the Jenig Complex: As visible in the BSE-images monazite appears as inclusions within A) staurolite and B) andalusite. Furthermore it has been observed within garnet and rock matrix. In general it is less than 50 µm in size.

### 9.1.2 Conditions and timing of the amphibolite facies event

Porphyroblast growth within the fine-grained matrix shows a general succession with garnet, followed by staurolite and finally andalusite, whereby the time spans of growth of these minerals might have been overlapping. Their growth is accompanied by the consumption, recrystallization and formation of chlorite, biotite and muscovite. However, the change in the mineral association clearly indicates increasing temperatures at low pressures, whereby the peak of metamorphism occurred at amphibolite-facies *P-T* conditions at 450 to 530°C and 0.24 to 0.42 GPa.

Timing of the amphibolites-facies event can be deduced from the Sm-Nd and monazite EMS-data. Nearly all age values calculated from the Sm-Nd analyses are in the range of 230-260 Ma, whereas all monazite EMS-data are 250-300 Ma (including the errors). Therefore it is evident that the low-pressure amphibolites-facies event occurred during Permian to Middle Triassic time. However, with the available data it is possible to argue for a more precise age information. EMS-monazite dating yielded ages in the range of 270-278 Ma, but the errors on the individual values are large. Furthermore the monazites grew during an undefined temperature interval on the prograde part of the *P-T* path.

The Sm-Nd analyses also allow space for interpretation: Even if all four whole rock powders yielded more or less the same results, the corresponding garnets show quiet different $^{147}Sm/^{144}Nd$ ratios. The $^{147}Sm/^{144}Nd$ ratios are negatively correlated with the Sm and Nd contents. Three of the four garnets fit well to a trend line whereas garnet separate of sample RS11/98 is situated above the line (Fig. 5). This implies contamination of the garnet separates with different amounts of REE-rich phases. These phases are at least partly monazite mentioned above and since monazite is not much older than the garnet its influence on the garnet age should be minor. The garnet fraction of sample RS11/98 which does not fit to the trend line has to contain an additional most probably older phase with a lower $^{143}Sm/^{144}Nd$ ratio, which has an obvious influence on the age value. For this reasons we calculated a pooled isochron from garnets and

| Sample | Sm [ppm] | Nd [ppm] | $^{147}Sm/^{144}Nd$ | $^{143}Nd/^{144}Nd \pm 2\sigma m$ | | $\varepsilon^0_{Nd}$ | $T^{Nd}DM$ |
|---|---|---|---|---|---|---|---|
| RS11/98 WR | 8.197 | 42.75 | 0.1159 | 0.511903 | 4 | -14.3 | 1.74E+09 |
| RS11/98 Grt | 1.813 | 6.165 | 0.1778 | 0.512049 | 5 | -11.5 | |
| RS11/98 St | 0.574 | 2.333 | 0.1487 | 0.511964 | 3 | -13.1 | |
| RS13/98 WR | 11.62 | 66.41 | 0.1057 | 0.511895 | 3 | -14.5 | 1.59E+09 |
| RS13/98 Grt | 0.839 | 1.123 | 0.4516 | 0.512468 | 13 | -3.3 | |
| RS13/98 St | 1.461 | 1.635 | 0.5403 | 0.512552 | 6 | -1.7 | |
| RS13/98 St2 | 1.577 | 2.702 | 0.3529 | 0.512290 | 3 | -6.8 | |
| RS36/00 WR | 10.21 | 52.40 | 0.1178 | 0.511911 | 5 | -14.2 | 1.75E+09 |
| RS36/00 Grt | 2.075 | 5.769 | 0.2174 | 0.512074 | 5 | -11.0 | |
| RS38/00 WR | 19.14 | 101.5 | 0.1141 | 0.511901 | 3 | -14.4 | 1.71E+09 |
| RS38/00 Grt | 2.479 | 8.244 | 0.1818 | 0.512014 | 3 | -12.2 | |

| Sample | Rb [ppm] | Sr [ppm] | $^{87}Rb/^{86}Sr$ | $^{87}Sr/^{86}Sr \pm 2\sigma m$ | |
|---|---|---|---|---|---|
| RS13/98 WR | 155.4 | 248.6 | 1.8133 | 0.72719 | 6 |
| RS13/98 Bt | 440.7 | 6.624 | 202.78 | 1.25178 | 6 |
| RS11/98 WR | 372.0 | 248.9 | 4.3356 | 0.73172 | 5 |
| RS11/98 Bt | 497.6 | 11.80 | 126.65 | 1.08974 | 16 |
| RS28/01 WR | 178.7 | 94.42 | 5.4977 | 0.74663 | 6 |
| RS28/01 Bt | 479.2 | 2.762 | 571.56 | 2.12305 | 34 |

**Table 4:** Sm-Nd and Rb-Sr data from Al-metapelites of the Jenig Complex and a metapelite from the garnet-staurolite mica schist zone near Kötschach (sample RS28/01).

WR's of samples RS13/98, RS36/00 and RS38/00. The result is 254±8 Ma with an MSWD of 3.2.

Based on the investigations of the thin sections staurolite formed partly contemporaneously but mostly later than the garnet. In fact one of the staurolite-WR ages is younger (231±4 Ma) than the pooled garnet isochron, whereas the other is the same within the error (244±4 Ma). However, it has to be mentioned that staurolite may have crystallised from a matrix which was slightly depleted in Sm, because of the former fractionation of Sm into the garnet.

Summarizing the data we conclude a Permian formation of the monazite, most probably on the prograde part of the *P-T* path. Garnet and staurolite subsequent grew under upper greenschist- respectively amphibolites-facies P-T conditions during late Permian to Early Triassic times (260-230 Ma).

### 9.1.3 Retrograde evolution and cooling history

The main part of the Jenig Complex shows only minor retrograde overprint. Data to reconstruct the cooling history are available in Schuster et al. (2001), following the blocking temperature concept by Jäger (1979): cooling below about 400 °C, the closure temperature of the K-Ar isotopic system in muscovite, occurred at 205±5 Ma in the Late Triassic. With respect to Ar-Ar ages of biotites 300 °C were reached at 185±3 Ma in the Early Jurassic (Fig. 7). Rb-Sr biotite data measured on the same biotite separates yield one age of 187±3 Ma which fits well with the Ar-Ar biotite ages whereas the second is older and yields 210±2 Ma (Fig. 8 A, 8B, recalculated with the decay constant form Nebel et al., 2011; $1.393\pm0.004\times10^{-11}$ $yr^{-1}$).

The observed long time span between metamorphic peak and cooling below 400°C and 300°C respectively, leads to the question if the data reflect cooling after the metamorphic peak, or after an additional and independent thermal pulse. To answer this question it is necessary to analyse the geotectonic environment and paleogeographic situation of the continental fragment forming the Austroalpine unit today during the time span of interest. According to Schuster and Stüwe (2008) the recent Austroalpine unit was in an extensional environment through Permian and Early Triassic times. Extension was compensated by lithospheric thinning until in the Anisian the Meliata Ocean as a part of the western Neotethys opened in the

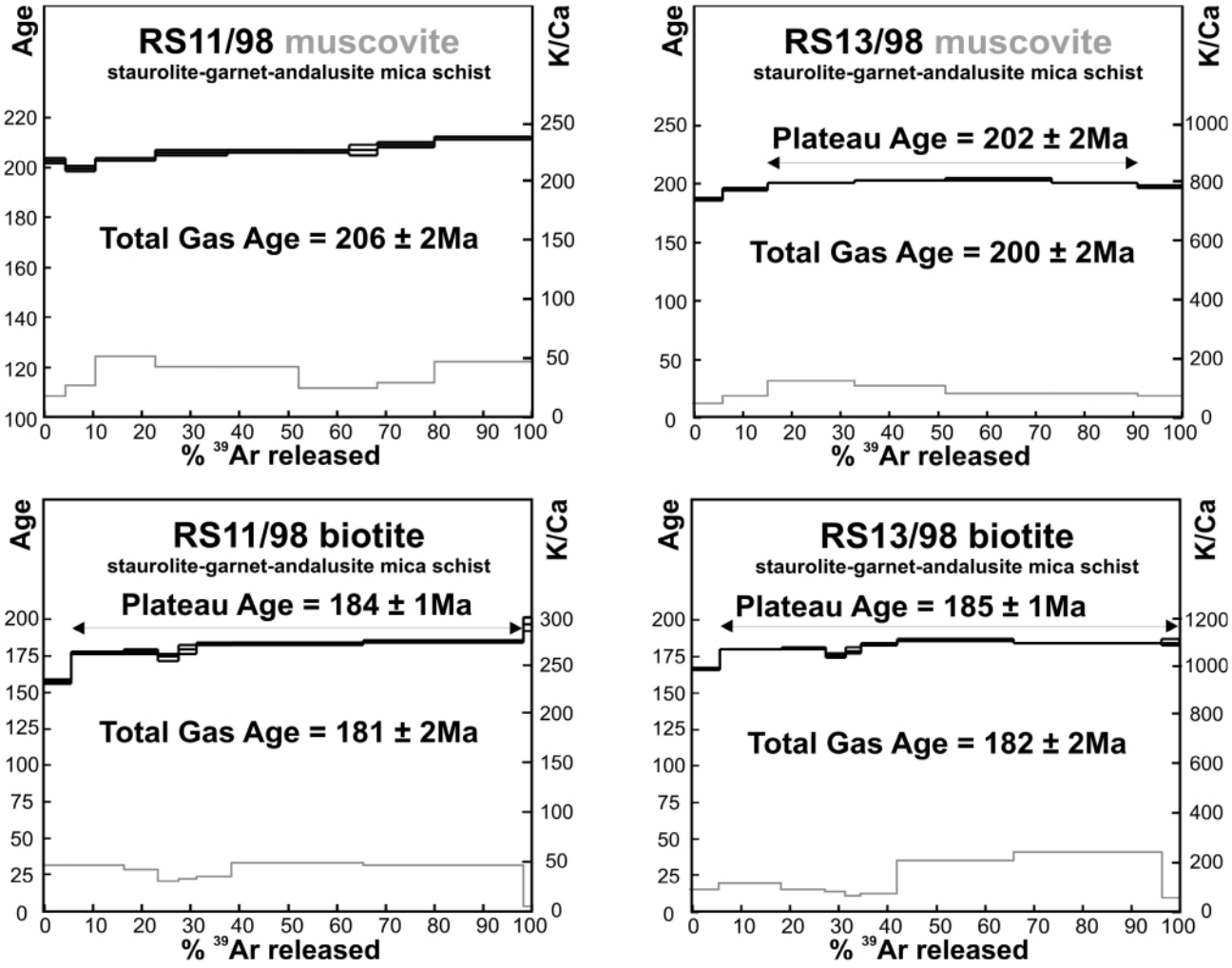


**Figure 7:** Ar-Ar diagrams of muscovite and biotite from the Jenig Complex (data from Schuster et al. 2001). The investigated micas have a grain size of 0.2-0.3 mm and represent porphyroblasts within the fine-grained matrix. The determined ages indicate cooling of the rocks below 400±50 °C and 300±50 °C at 205±5 Ma and 180±50 Ma respectively (following the blocking temperature concept by Jäger, 1979).

southeast. Since then the recent Austroalpine unit formed a segment at the northwestern shelf of this oceanic realm. The whole area was at sea level and up to 3250 m of mostly shallow water sediments were deposited onto it. Magmatic activity can be recognised from the early Permian until the early Late Triassic at about 225 Ma (Thöni and Miller, 2000; Schuster et al, 2001). In the Early Jurassic extension continued and lead to the opening of the Penninic Ocean in the north. With respect to Manatschal et al. (2002) the initial parts of the Penninic Ocean floor were formed by subcontinetal mantle, which was exhumed along a south dipping normal fault from below the recent Austroalpine unit. During this process a thermal pulse in the crust might have produced by upwelling of astenospheric mantle.

Due to this geodynamic evolution a thermal pulse at about 210 Ma causing a rejuvenation of the K-Ar isotopic system in muscovite seems to be unlikely. More likely muscovite and biotite ages reflect continuous cooling after the metamorphic peak in the Permian to Early Triassic. This cooling is not related to exhumation, but due to relaxation of the isotherms from a high geothermal gradient at the peak of metamorphism to a lower gradient in Early Jurassic time. During this time span the investigated rocks stayed within the upper part of the middle crust. The thermal relaxation triggered deposition of up to 3250 m of sediments on top of the slowly subsiding lithosphere.

### 9.1.4 Lithostratigraphic definition of the Jenig Complex

In the subdivision by Heinisch et al. (1983) the lithologies described in this paper are part of the zone of (un)metamorphosed Paleozoic rocks. However, these metapelites and metapsamites and the incooperated andalusite-quartz vains form a characteristic association which can be mapped and separated from the surrounding (Schönlaub, 1987). Further it is characterised by a monophase tectonometamorphic evolution. At present the time of deposition and the internal stratigraphy of the rock series is unknown, it may be upright or inverted. Therefore this volume of rocks is not a lithostratigraphic unit in the proper sense but a lithodemic unit (North American Stratigraphic Code 2005; Concept Definition Task Group CGI/IUGS 2008, Schiegl et al. 2009). With respect to the lithodemic nomenclature a series of rock consisting of one class of rocks (e.g. metamorphic or magmatic) has to be attributed as lithodem whereas when both classes are present it is a complex. The investigated rock series is composed of metapelites but the intercalated andalusite-bearing quartz-veins formed by segregation can not be classified as metasedimentary rocks. Therefore we suggest a classification as complex. The name of a lithodemic unit includes a geographic name (type locality) and the lithodemic rank and we propose the name Jenig Complex.

### 9.1.5 Tectonic position of the Jenig Complex

The Jenig Complex forms part of the pre-Mesozoic crystalline basement at the northern slops of the Gail valley. Based on the available data this basement consists of several parts

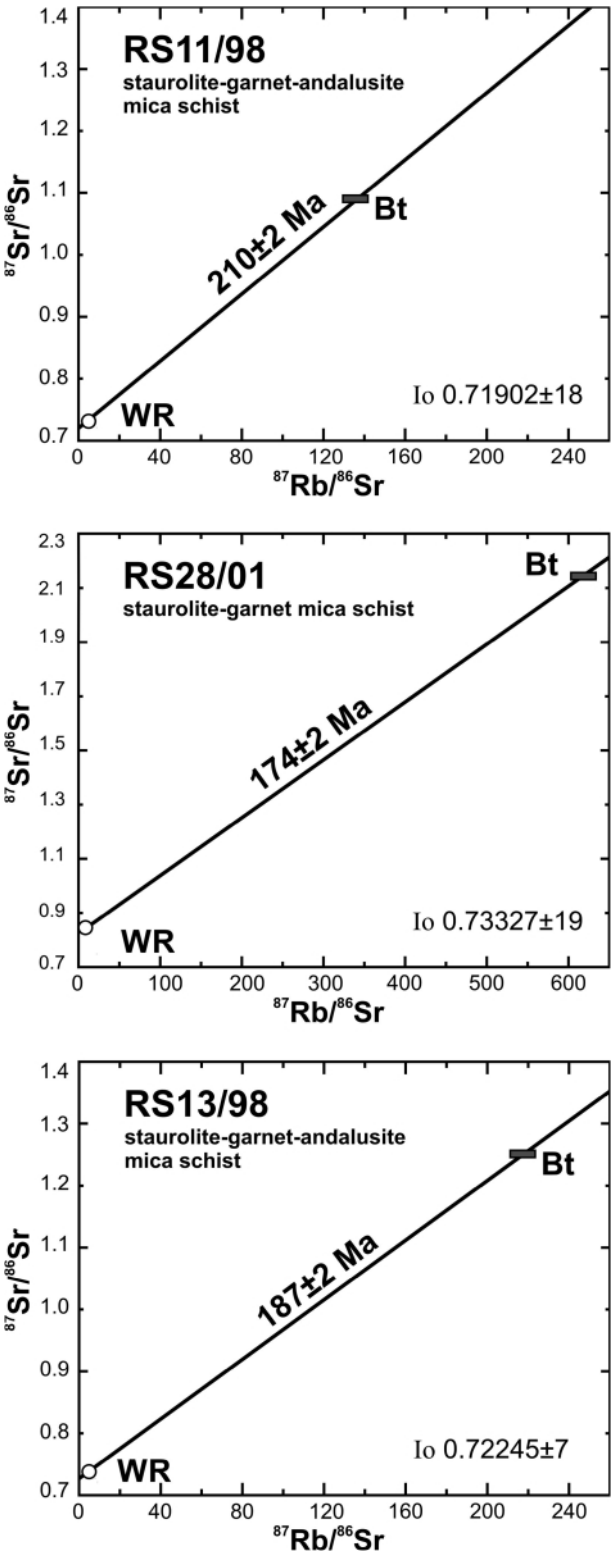


**Figure 8:** Rb-Sr age diagrams for two biotits from the Jenig Complex and one biotite from the garnet-staurolite mica schist zone near to Kötschach. All age values range from Late Triassic to Early Jurassic. Although the blocking temperature for the Rb-Sr system in biotite is lower than for K-Ar in muscovite the ages are in the same range. Therefore the determined ages can not be interpreted to reflect Variscan ages partly reset during the eo-Alpine (Cretaceous) event.

which experienced variable metamorphic grades at different times (Fig. 9): as indicated by an Ar-Ar muscovite age of 315 Ma (Neubauer and Genser 2009) the mica schists and paragneisses of the garnet-mica schist zone were formed and cooled down during the Variscan tectonometamorphic event. Most probably the amphibolite-facies assemblage in the staurolite-garnet mica schist zone developed at the same time. In contrast the Jenig Complex underwent the major metamorphic overprint during the Permo-Triassic extensional event. These differences clearly indicate that the crystalline basement at the northern slopes of the Gail valley is neither a continuous tectonic unit nor a lithostratigraphic unit but consists of several tectonic slices. One of these slices is formed by the Jenig Complex. Therefore terms like "Gailtalkristallin" (Heinisch et al. 1984, Heinisch 1987) or "Gailtal Crystalline Complex" (Neubauer et al. 1999) suggesting a homogeneous lithostratigraphic or tectonic unit are problematic.

Also the Ar-Ar muscovite and Rb-Sr biotite ages, indicating cooling below 400°C and 300°C respectively are not homogeneous in the study area. In the garnet mica schist zone and the adjacent northern parts of the phyllonite zone Carboniferous ages of 310-315 Ma can be related to the Variscan tectonometamorphic event. In southern parts of the phyllonite zone, bordering to the staurolite-garnet mica schist zone Early Jurassic ages have been found, arguing for recrystallization during shearing in Jurassic time (Neubauer and Genser 2009). The Rb-Sr biotite age from the staurolite-garnet mica schist zone presented in this paper yielded also a Jurassic age value. This value might be due to partly rejuvenation of a Variscan age by a weak Cretaceous overprint (at less than 300°C) or due to cooling in the Jurassic. However, since also the Rb-Sr biotite ages from the Jenig Complex are in the same range the second possibility is more likely.

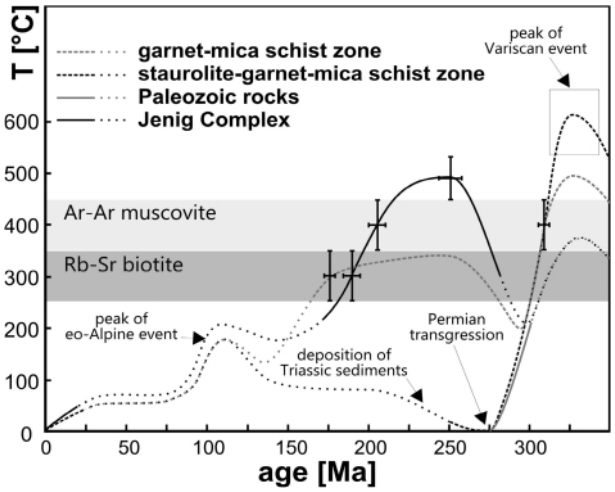


**Figure 9:** *T-t* paths for the different parts of the Austroalpine crystalline basement at the northern slopes of the Gail valley. (1) Rocks from the garnet-mica schist zone experienced an upper greenschist-facies metamorphism during the Variscan event. They are not directly overlain by Permian sediments and show a final cooling below 300 °C in the Early Jurassic. (2) Amphibolite-facies conditions were reached in the staurolite-garnet-mica schist zone during the Variscan event. After that the rocks were exhumed and transgressed by Permian sediments. (3) The Paleozoic unit is characterised by a Variscan lower greenschist-facies imprint and is overlain by Permian sediments. (4) In contrast the Jenig Complex experienced an amphibolite metamorphism in Permian to the Early Triassic. Since these four units show distinctly different *T-t* paths they clearly represent four individual tectonic units. The term "Gailtalkristallin" is whether neither tectonic nor lithostratigraphic, but just a summary of crystalline rocks in a geographic area.

In any case temperatures during the eo-Alpine tectonometamorphic event in the Cretaceous were low (<300°C) in all parts of the crystalline basement. This is in agreement with the data from the overlying Permo-Mesozoic sediments, which reached maximum (lower) anchizonal conditions (Rantitsch 2001). Therefore Neubauer and Genser (2009) concluded that the lower greenschist-facies, sinistral phyllonite zones (Heinisch 1987; Unzog 1989) formed prior to the Cretaceous and mainly during the Jurassic. They may have formed during the amalgamation of the four parts of the Drau Range which are characterised by different facies evolutions (Lein et al. 1997). With respect to the overall facies distribution of the Austroalpine Triassic sediments (Tollmann, 1977, 1985) a Jurassic sinisdral strike slip fault system to the north of the recent Periadriatic fault was postulated by Bechstädt (1978) and later on by other authors (Schuster and Frank 2000; Schmid et al. 2004). During the eo-Alpine tectonothermal event the whole area between the Periadriatic fault and the recent Tauern Window was folded by E-W trending axes. This folding is responsible for the preservation of the Permo-Mesozoic sediments of the Drau Range which occur in a large scale syncline. Finally, brittle deformation in the Cretaceous and/or Cenozoic shearing along the Periadriatic fault caused the formation of pseudotachyllites (Heinisch and Spengler 1988).

## 10. Conclusions

Investigations on the crystalline rocks north of Jenig constrain the following results:

- The mica schists, quarzitic mica schists, paragneisses, quartzites, garnet- and amphibole-bearing quartzschists described in this paper experienced a unique metamorphic evolution. They are characterised by a prograde metamorphic imprint and contemporaneous formation of andalusite-bearing quartz veins.
- Mica schists developed from Al-rich pelites show greenschist-facies assemblage with fine-grained white mica, biotite, chlorite and quartz. During prograde metamorphism this assemblage was successively overgrown by garnet, staurolite and andalusite porphyroblast which formed together with coarse-grained biotite and muscovite flakes. Peak metamorphic conditions reached 450 to 530°C and 0.24 to 0.42 GPa.
- EMS-dating of monazite indicates formation of this mineral at the prograde part of the *P-T-t* path at 275±25 Ma. The amphibolite-facies peak assemblage formed at 254±8 Ma, based on a Sm-Nd isochron age.
- With respect to Ar-Ar and Rb-Sr data on muscovites and biotites final cooling below 400°C and 300°C occurred at 205±5 Ma (Late Triassic) and 185±5 Ma (Early Jurassic)

respectively. Cooling is due to the relaxation of isotherms and not due to exhumation of the rocks.

- Due the occurrence north of Jenig and a composition with metamorphic and possibly magmatic (andalusite-bearing quartz veins) rocks we suggest to formalise the investigated rock series as a lithodemic unit with the name Jenig Complex.
- The Jenig Complex forms a tectonic slice which was formed by Jurassic sinistal strike-slip tectonics, Cretaceous folding and finally Cenozoic exhumation by shearing along the Periadriatic fault.

## Acknowledgements

We gratefully acknowledge Richard Tessadri for performing whole rock XRF analyses. Manfred Linner and Monika Horschinegg is thanked for their help to determine the Sr- and Nd-isotopic data. Many thanks to Thorsten Nagel and Christoph Hauzenberger for their constructive review which helped to improve the manuscript. Financial support for the fieldwork through the Austrian Science Foundation (projects Nr. P12277 and P14525) is kindly acknowledged.

## References

Amanti, M., Bontempo, R., Cara, P., Conte, G., Di Bucci, D., Lembo, P., Pantaleone, N.A. and Ventura, R. (eds) 2001. Carta geologica d'Italia Interattiva Geological Map of Italy, 1:100000 SGN, SSN, ANAS.3 CD-rom.

Anderle, N., 1977. Geologische Karte der Republik Österreich 1:50.000, Blatt 200 Arnoldstein, Geologische Bundesanstalt, Wien.

Bögel, H., Morteani, G., Sassi, F.P., Satir, M. and Schmidt, K., 1979. The Herzynian and pre-Herzynian Development of the Eastern Alps, Report on a Meeting. Neues Jahrbuch Geologie Paläontologie Abhandlungen, 159/1, 87-112.

Bestel, M., Gawronski, T., Abart, R. and Rhede, D., 2009. Compositional zoning of garnet porphyroblasts from the polymetamorphic Wölz Complex, Eastern Alps. Mineralogy and Petrology, 97/3-4, 173-188. http://dx.doi.org/10.1007/s00710-009-0084-z

Gaidies, F., Abart, R., DeCapitani, C., Schuster, R., Connolly, J. A.D. and Reusser, E., 2006. Characterisation of polymetamorphism in the Austroalpine basement east of the Tauern Window using garnet isopleth thermobarometry. Journal of Metamorphic Geology, 24, 451-475. http://dx.doi.org/10.1111/j.1525-1314.2006.00648.x

Garcia, D., Coelho, M. and Perrin, M., 1991. Fractionation between $TiO_2$ and Zr as a measure of sortine within shale and sandstone series (Northern Portugal). European Journal of Mineralogy, 3, 401-414. http://dx.doi.org/10.1127/ejm/3/2/0401

Habler, G. and Thöni, M., 2001. Preservation of Permo-Triassic low-pressure assemblages in the Cretaceous high-pressure metamorphic Saualpe crystalline basement (Eastern Alps, Austria). Journal of Metamorphic Geology, 19, 679-697. http://dx.doi.org/10.1046/j.0263-4929.2001.00338.x

Heinisch, H., 1987. Concepts for the geological evolution of Gailtalkristallin (Kärnten – Austria). In: Flügel, H.W., Sassi, F. P. and Grecula, P. (eds), Pre-Variscan and Variscan events in the Alpine-Mediteranian mountain belt. Mineralia slovaca – Monography, Alfa, Bratislava pp. 293-312.

Heinisch, H., Schmidt, K. and Schuh, H., 1983. Zur geologischen Geschichte des Gailtalkristallins im unteren Lesachtal westlich von Kötschach-Mauthen (Kärnten, Österreich). Jahrbuch der Geologischen Bundesanstalt, 126/4, 477-486.

Heinisch, H. and Spengler, W., 1988. Mehrphasige Deformation und Pseudotachylitbildung im Gailtalkristallin und am Periadriatischen Lineament zwischen Sillian und Kötschach-Mautern (Osttirol/Kärnten, Österreich). Erlanger geologische Abhandlungen, 116, 41-52.

Henry, D.J., Guidotti, C.V. and Thomson, J.A., 2005. The Ti-saturation surface for low-to-medium pressure metapelitic biotites: implications for geothermometry and Ti-substitution mechanisms. American Mineralogist, 90, 316-328. http://dx.doi.org/10.2138/am.2005.1498

Heritsch, H. and Paulitsch, P., 1958. Erläuterungen zur Karte des Kristallins zwischen Birnbaum und Pressegger See, Gailtal. Jahrbuch der Geologischen Bundesanstalt, 101, 191-200.

Hoinkes, G., Koller, F., Rantitsch, G., Dachs, E., Höck, V., Neubauer, F. and Schuster, R., 1999. Alpine metamorphism of the Eastern Alps. Schweizer Mineralogisch Petrographische Mitteilungen, 79, 155-181.

Holland, T.J.B. and Powell, R., 1998. An internally-consistent thermodynamic data set for phases of petrological interest. Journal of Metamorphic Geology, 8, 89-124. http://dx.doi.org/10.1111/j.1525-1314.1990.tb00458.x

Jäger, E., 1979. Introduction to Geochronology. In: E. Jäger and J.C. Hunziger (eds.), Lectures in Isotope Geology, Springer, Berlin Heidelberg New York, pp. 1-12. http://dx.doi.org/10.1007/978-3-642-67161-6_1

Janàk, M., Froitzheim, N., Luptàk, B., Vrabec, M. and Krogh Ravna, E.J., 2004. First evidence for ultrahigh-pressure metamorphism in Pohorje, Slovenia: Tracing deep continental subduction in the Eastern Alps. Tectonics, 23 , TC5014. http://dx.doi.org/10.1029/2004TC001641

Kober, L., 1938. Der geologische Aufbau Österreichs. Springer, Wien, 204 pp.

Lein, R., Gawlick, H.-J. and Krystyn, L., 1997. Paläogeographie und tektonische Herkunft des Drauzuges - Eine Diskussion auf der Basis von Fazies- und Conodont Colour Alteration Index (CAI)-Untersuchungen. Zentralblatt Geologie Paläontologie, Teil I 5/6, 471-483. the Eastern Alps. – Tschermaks Mineralogisch Petrographi-sche Mitteilungen, 22, 175-199.

Ludwig, K.R. 2003. Isoplot/Ex version 3.0. A geochronological toolkit for Microsoft Excel. Berkeley Geochronological Centre Special Publication, Berkeley, 70 pp.

Manatschal, G., Müntener, O., Bernoulli, D. and Desmurs, L., 2002. Birth and Early Evolution of Alpine Ocean Basins: Evidence of remnants of an Ocean-Continent-Transition Preserved in the Totalp, Err-Platta and Malenco units in SE-Wwitzerland and N-Italy (Central Alps). Field Guide Swiss Academy of Natural Sciences 2002 (Davos), 52 pp.

Nebel, O., Mezger, K., and Scherer, E.E., 2011. Re-evaluation of the Rubidium decay constant by age comparison against the U-Pb system. Earth and Planetary Science Letters, 301, 1-8. http://dx.doi.org/10.1016/j.epsl.2010.11.004

Neubauer, F., Hoinkes, G., Sassi, F.P., Handler, R., Höck, V., Koller, F. and Frank, W., 1999. Pre-Alpine metamorphism in the Eastern Alps. Schweizer Mineralogisch Petrographische Mitteilungen, 79, 41-62.

Neubauer, F. and Genser, G., 2009. Metamorphic and structural evolution of the Gailtal basement complex: significance for Austroalpine tectonics in Eastern Alps. Abstract Volume 9th Workshop on Alpine Geological Studies Cogne/Italy 16.-18. September 2009.

Nowak, H.W. 1983. Zur Metamorphose und Struktur des Kristallin im Lesachtal/Kärnten unter besonderer Berücksichtigung baugeologischer Gesichtspunkte. Unpublished Report, Geologische Bundesanstalt, Wien, 89 pp.

Paulitsch, P., 1960. Das Kristallin zwischen Tassenbach und Obertilliach, Osttirol, und seine Metamorphose. Verhandlungen der Geologischen Bundesanstalt, 1960, 103-119.

Philippitsch, R., Malecki, G. and Heinz, H., 1986. Andalusit-Granat-Staurolith-Glimmerschiefer im Gailtalkristallin (Kärnten). Jahrbuch der Geologischen Bundesanstalt, 129/1, 93-98.

Powell, R., Holland, T.J.B., 2003. Course Notes for "Petrological Thermodynamics Short Course". (ETH, Zurich) on CD-ROM.

Probst, G., Brandner, R., Hacker, P., Heiss, G. and Prager, Ch., 2003. Hydrogeologische Grundlagenstudie Westliche Gailtaler Alpen/Lienzer Dolomiten (Kärnten/Osttirol). Beiträge zur Hydrogeologie, 54, 5-62.

Purtscheller, F. and Sassi, F.P., 1975. Some thoughts on the pre-Alpine metamorphic history of the Austridic basement of the Eastern Alps. – Tschermaks Mineralogisch Petrographische Mitteilungen, 22, 175-199.

Rantitsch, G., 2001. Thermal history of the Drau Range (Eastern Alps). Schweizer Mineralogisch Petrographische Mitteilungen, 81, 181-196.

Schiegl, M., Schuster, R., Krenmayr, H.G., Lipiarski, P., Pestal, G., Stöckl, W. and Untersweg, T., 2009. GeoSciML - ein konzeptionelles Datenmodell für die Geologie? Jahrbuch der Geologischen Bundesanstalt, 148/2, 213-226.

Schmid, S.M., Fügenschuh, B., Kissling, E. and Schuster, R., 2004. Tectonic map and overall architecture of the Alpine orogen. Eclogae Geolgae Helveticae, 97/1, 93-117. http://dx.doi.org/10.1007/s00015-004-1113-x

Schönlaub, H.P., 1979. Das Paläozoikum in Österreich. Verbreitung, Stratigraphie, Korrelation, Entwicklung und Paläogeographie nicht metamorpher und metamorpher Abfolgen. Abhandlungen der Geologischen Bundesanstalt, 33, 124 pp.

Schönlaub, H.P., 1985. Geologische Karte der Republik Österreich 1:50.000, Blatt 197 Kötschach, Geologische Bundesanstalt, Wien.

Schönlaub, H.P., 1987. Geologische Karte der Republik Österreich 1:50.000, Blatt 198 Weisspriach, Geologische Bundesanstalt, Wien.

Schönlaub, H.P., 1989. Geologische Karte der Republik Österreich 1:50.000, Blatt 199 Hermagor, Geologische Bundesanstalt, Wien.

Schönlaub, H.P., 1997. Geologische Karte der Republik Österreich 1:50.000, Blatt 196 Obertilliach, Geologische Bundesanstalt, Wien.

Schönlaub, H.P., 2000. Geologische Karte der Republik Österreich 1:50.000, Blatt 195 Sillian, Geologische Bundesanstalt, Wien.

Schuster, R., Koller, F., Hoeck, V., Hoinkes, G. and Bousquet, R., 2004. Metamorphic evolution of the Eastern Alps. Mitteilungen der Österreichischen Mineralogischen Gesellschaft, 149, 175-199.

Schuster, R., Scharbert, S., Abart, R. and Frank, W., 2001. Permo-Triassic extension and related HT/LP metamorphism in the Austroalpine - Southalpine realm. Mitteilungen der Geologie und Bergbaustudenten Österreichs, 44, 111-141.

Schuster, R. and Stüwe, K. 2008. The Permian Metamorphic Event in the Alps. Geology, 36/8, 303-306. http://dx.doi.org/10.1130/G24703A.1

Schuster, R. and Thöni, M., 1996. Permian Garnet: Indications for a regional Permian metamorphism in the southern part of the Austroalpine basement units. Mitteilungen der Österreichischen Mineralogischen Gesellschaft, 141, 219-221.

Sölva, H., Grasemann, B., Thöni, M., Thiede, R., and Habler, G., 2005. The Schneeberg Normal Fault Zone: Normal faulting associated with Cretaceous SE- directed extrusion in the Eastern Alps (Italy/Austria). Tectonophysics, 401, 143-166. http://dx.doi.org/10.1016/j.tecto.2005.02.005

Stampfli, G.M. and Borel, G.D., 2004. The Transmed Transsects in Space and Time: Constraints on the Paleotectonic Evolution of the Mediteranian Domain. In: Cavazza W, Roure F, Spakman W, Stampfli GM, and Ziegler PA (eds): The TRANSMED Atlas: the Mediterranean Region from Crust to Mantle, Springer, Berlin, 141 pp.

Steidl, M., Tropper, P., Linner, M. and Schuster, R., 2010. Petrology of the polymetamorphic metapelites from the Michelbach Complex (Defereggen Complex, East Tyrol). Journal of Alpine Geology, Abstract PANGEO 2010 Leoben, Wien, 52, 235.

Steininger, F.F. and Piller, W.E., 1999. Empfehlungen (Richtlinien) zur Handhabung der stratigraphischen Nomenklatur. Cou-rier Forschungsinstitut Senkenberg, 209, 1-19.

Stüwe, K. and Schuster, R. 2010. Initiation of Subduction in the Alps: Continent or Ocean? Geology, 38/2, 175-178. http://dx.doi.org/10.1130/G30528.1

Symmes, G.H. and Ferry, J.M., 1991. Evidence from mineral assemblages for infiltration of pelitic sshists by aqueous fluids during metamorphism. Contributions to Mineralogy and Petrology, 108, 419-438. http://dx.doi.org/10.1007/BF00303447

Thöni, M., 1999. A review of geochronological data from the Eastern Alps. Schweizer Mineralogisch Petrographische Mitteilungen, 79/1, 209-230.

Thöni, M. and Miller, Ch., 2000. Permo-Triassic pegmatites in the eo-Alpine eclogite-facies Koralpe complex, Austria: age and magma source constraints from mineral chemical, Rb-Sr and Sm-Nd isotopic data. Schweizer Mineralogisch Petrographische Mitteilungen, 80, 169-186.

Thöni, M. and Miller, Ch., 2009. The "Permian event" in the Eastern European Alps: Sm-Nd and P.-T data recorded by multi-stage garnet from the Plankogel unit. Chemical Geology, 260, 20-36. http://dx.doi.org/10.1016/j.chemgeo.2008.11.017

Tollmann, A., 1963. Ostalpensynthese. Deuticke, Wien, 256 pp.

Tollmann, A., 1977. Geologie von Österreich. Band 1. Die Zentralalpen. Deuticke, Wien, 766 pp.

Tollmann, A., 1985. Geologie von Österreich. Band 2. Außerzentralalpiner Anteil. Deuticke, Wien, 710 pp.

Unzog, W., 1989a. Schertektonik im Gailtalkristallin und seiner Begrenzung. PhD thesis, Faculty of Science, University of Graz, Austria, Graz, 204 pp.

Unzog, W., 1989b. Mineralzation in a brittle-ductile shearzone: examples from the Gailtalkristallin, Austria. Terra Abstracts, 79th Annual Meeting of the Geologische Vereinigung: Mineral Deposits 1/2, 46.

Unzog, W., 1991. Alpidic left-lateral strike-slip tectonics in the Gailtal crystalline, Austria. Terra Abstracts, 6th Meeting of the European Union of Geosciences, 3/1: 251.

Unzog, W., 1992. Stress and strain in the metamorphic Gailtal Complex, Eastern Alps. Terra abstracts Supplement, 2, 68.

Received: 31 March 2014
Accepted: 29 September 2014

Ralf SCHUSTER[1)*], Peter TROPPER[2)], Erwin KRENN[3)], Friedrich FINGER[3)], Wolfgang FRANK[4)] & Rudolf PHILIPPITSCH[5)]

[1)] Geologische Bundesanstalt, Neulinggasse 38, A-1030 Wien, Austria;

[2)] Institut für Mineralogie und Petrographie, Fakultät für Geo- und Atmosphärenwissenschaften, Universität Innsbruck, Innrain 52f, A-6020 Innsbruck, Austria;

[3)] Fachberich Materialforschung und Physik, Universität Salzburg, Hellbrunnerstrasse 34, 5020 Salzburg, Austria;

[4)] Köhldorfergasse 26, 3040 Neulengbach, Austria;

[5)] Jadersdorf 18, 9620 Hermagor, Austria;

[*)] Corresponding author, ralf.schuster@geologie.ac.at